3 Continuation Power Flow

3.1 Introduction

As mentioned in the previous chapter, the continuation method is a mathematical path-following methodology used to solve systems of nonlinear equations. The numerical derivation of this method is shown in [1]. Using the continuation method, we can track a solution branch around the turning point without difficulty. This makes the continuation method quite attractive in approximations of the critical point in a power system. The continuation power flow captures this path-following feature by means of a predictor-corrector scheme that adopts locally parameterized continuation techniques to trace the power flow solution paths. The next sections explain the principles of continuation power flow.

3.2 Locally Parameterized Continuation

A parameterization is a mathematical means of identifying each solution on the branch, a kind of measure along the branch. When we say "branch," we refer to a curve consisting of points joined together in $n+1$ dimensional space that are solutions of the nonlinear equations

$$F(x,\lambda) = 0 \tag{3.1}$$

This equation is obtained by introducing a load parameter, λ, into the original system of nonlinear equations, $F(x) = 0$. For a range of values of λ, it is quite possible to identify each solution on the branch in a mathematical way [2]. But not every branch can be parameterized by an arbitrary parameter. The solution of Eq.3.1 along a given path can be found for each value of λ, although problems arise when a solution does not exist for some maximum possible λ value. At this point, one of the

state variables, x_i, can be used effectively as the parameter to be varied, choice of which is determined locally at each continuation step. Thus, the method is designated as the locally parameterized continuation. In summary, local parameterization allows not only the added load parameter λ, but also the state variables to be used as continuation parameters.

3.3 Formulation of Power Flow Equations

To apply locally parameterized continuation techniques to the power flow problem, the power flow equations must be reformulated to include a load parameter, λ. This reformulation can be accomplished by expressing the load and the generation at a bus as a function of the load parameter, λ. Thus, the general forms of the new equations for each bus i are

$$\Delta P_i = P_{Gi}(\lambda) - P_{Li}(\lambda) - P_{Ti} = 0 \tag{3.2}$$

$$\Delta Q_i = Q_{Gi} - Q_{Li}(\lambda) - Q_{Ti} = 0 \tag{3.3}$$

where

$$P_{Ti} = \sum_{j=1}^{n} V_i V_j y_{ij} \cos(\delta_i - \delta_j - \gamma_{ij})$$

$$Q_{Ti} = \sum_{j=1}^{n} V_i V_j y_{ij} \sin(\delta_i - \delta_j - \gamma_{ij})$$

and $0 \le \lambda \le \lambda_{critical}$. $\lambda = 0$ corresponds to the base case, and $\lambda = \lambda_{critical}$ to the critical case. The subscripts L, G and T respectively denote bus load, generation, and injection. The voltage at bus i is $V_i \angle \delta_i$, and $y_{ij} \angle \gamma_{ij}$ is the $(i,j)^{th}$ element of the system admittance matrix $[y_{BUS}]$.

To simulate different load change scenarios, the P_{Li} and Q_{Li} can be modified as

$$P_{Li}(\lambda) = P_{Li0} + \lambda[K_{Li} S_{\Delta BASE} \cos(\psi_i)] \tag{3.4}$$

$$Q_{Li}(\lambda) = Q_{Li0} + \lambda[K_{Li} S_{\Delta BASE} \sin(\psi_i)] \tag{3.5}$$

where $S_{\Delta BASE}\cos(\Psi_i) = P_{Li0}$ and $Q_{Li0} = S_{\Delta BASE}\sin(\Psi_i)$.
Let $Q_{Li0} = P_{Li0}\tan(\Psi_i)$, then Eqs.3.4 and 3.5 can be rewritten as

$$P_{Li}(\lambda) = P_{Li0}[1+\lambda K_{Li}]$$

$$Q_{Li}(\lambda) = P_{Li0}\tan(\Psi i)[1+\lambda K_{Li}]$$

where

- P_{Li0}, Q_{Li0} = original load at bus i, active and reactive respectively;
- K_{Li} = multiplier designating the rate of load change at bus i as λ changes;
- ψ_i = power factor angle of load change at bus i;
- $S_{\Delta BASE}$ = apparent power, which is chosen to provide appropriate scaling of λ.

The active power generation can be modified to

$$P_{Gi}(\lambda) = P_{Gi0}(1+\lambda K_{Gi}) \tag{3.6}$$

where

- P_{Gi0} = active generation at bus i in the base case;
- K_{Gi} = constant specifying the rate of change in generation as λ varies.

Now if F is used to denote the entire set of equations, then the problem can be expressed as a set of nonlinear algebraic equation represented by Eq.3.1, with $x = [\underline{\delta}, \underline{V}]^T$. The predictor corrector continuation process can then be applied to these equations.

3.4 The Predictor-corrector Process

The first task in the predictor process is to calculate the tangent vector. This can be obtained from

$$[\underline{F}_\delta, \underline{F}_v, \underline{F}_\lambda] \begin{bmatrix} d\underline{\delta} \\ d\underline{V} \\ d\lambda \end{bmatrix} = 0$$

On the left side of the equation is a matrix of partial derivatives multiplied by the vectors of differentials. The former is the conventional power flow Jacobian augmented by one column (F_λ), whereas the latter $T = [d\underline{\delta}, d\underline{V}, d\lambda]^T$ is the tangent vector being sought. Normalization must be imposed to give $\underline{t}$ a nonzero length. One can use, for example

$$e_k^T \underline{t} = t_k = 1$$

where e_k is an appropriately dimensioned row vector with all elements equal to zero except the k^{th}, which is equal to one. If the index k is chosen properly, letting $t_k = \pm 1.0$ imposes a nonzero norm on the tangent vector and guarantees that the augmented Jacobian will be nonsingular at the point of maximum possible system load [3]. Thus, the tangent vector is determined as the solution of the linear system

$$\begin{bmatrix} \underline{F}_\delta & \underline{F}_v & \underline{F}_\lambda \\ & e_k & \end{bmatrix} [\underline{t}] = \begin{bmatrix} 0 \\ \pm 1 \end{bmatrix} \tag{3.7}$$

Once the tangent vector has been found by solving Eq.3.7, the prediction can be made as

$$\begin{bmatrix} \underline{\delta}^* \\ \underline{V}^* \\ \lambda^* \end{bmatrix} = \begin{bmatrix} \underline{\delta} \\ \underline{V} \\ \lambda \end{bmatrix} + \sigma \begin{bmatrix} d\underline{\delta} \\ d\underline{V} \\ d\lambda \end{bmatrix}$$

where '*' denotes the predicted solution, and σ is a scalar designating step size.

After the prediction is made, the next step is to correct the predicted solution. As mentioned in Chapter 2, the technique used here is local parameterization, whereby the original set of equations is augmented by one equation specifying the value of one of the state variables. In equation form, this relation is expressed as

$$\begin{bmatrix} F(\underline{x}) \\ x_k - \eta \end{bmatrix} = 0, \qquad x = \begin{bmatrix} \underline{\delta} \\ \underline{V} \\ \lambda \end{bmatrix}$$

where η is an appropriate value for the k^{th} element of x. Once a suitable index k and the value of η are specified, a slightly modified N-R power flow method (altered only by one additions equation and one additional state variable) can be used to solve the set of equations. This procedure provides the corrector needed to modify the predicted solution found in the previous section.

3.4.1 Selecting the continuation parameter

The best method of selecting the correct continuation parameter at each step is to select the state variable (change the underlined to variable) with the largest tangent vector component. In short, we select the state variable (change the underlined to variable) evidencing the maximum rate of change near a given solution. To begin with, λ is a good choice, and subsequent continuation parameters can be evaluated as:

$$x_k : |t_k| = \max\{|t_1|, |t_2|, \cdots, |t_m|\} \tag{3.8}$$

Here, $\underline{t}$ is the tangent vector. After the continuation parameter is selected, the proper value of either +1 or -1 should be assigned to t_k in the tangent vector calculation.

3.4.2 Identifying the critical point

To find the stopping criterion for the continuation power flow, we must determine whether the critical point has been reached. This can be done easily because the critical point is the point at which maximum loading (and hence maximum λ) occurs before decreasing. For this reason, at the critical point, the tangent vector component corresponding to λ (which is $d\lambda$) is zero and becomes negative once it passes the critical point. Thus, the sign of the $d\lambda$ component tells us whether the critical point has been passed or not.

The previous paragraphs summarize the basic continuation power flow. More details can be found in [4].

3.5 Examples

Two bus example: constant power load: the above approach is first demonstrated through a simple two bus example as shown in Fig.3.1.

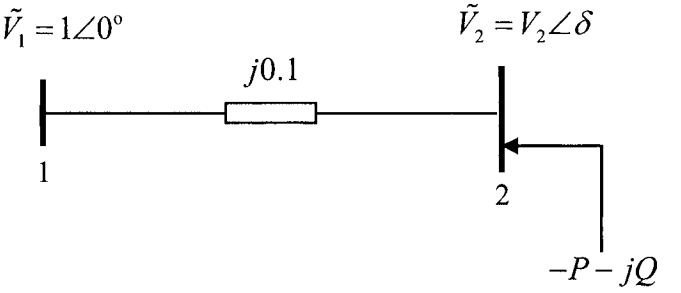

Fig.3.1 Two bus system

For this two bus example, the power flow equation at bus 2 can be formulated as:

$$(-P - jQ)^* = V_2\angle -\delta(Y_{21}V_1\angle\theta_{21} + Y_{22}V_2\angle\delta)$$

Suppose

- The voltage at the generator bus is: $\tilde{V}_1 = 1\angle 0$
- The voltage at the load bus is: $\tilde{V}_2 = V_2\angle\delta$
- The load is: $P + jQ$, so the injected power is: $-P - jQ$
- The load power factor keeps constant.

By introducing parameters λ and K, we can represent load increase scenario at bus 2 as follows:

$$P = P_0 * (1 + \lambda K)$$
$$Q = Q_0 * (1 + \lambda K)$$

where $Q_0 = P_0 * \tan(\psi)$ and is the constant load changing factors specified for bus 2.

Then we get two equations corresponding to real power and reactive power:

$$0 = P_0 * (1 + \lambda K) + Y_{21} V_2 \cos(\theta_{21} - \delta) + Y_{22} V_2^2 \cos(\theta_{22}) = f_1(\delta, V_2, \lambda) \quad (3.9)$$

$$0 = Q_0 * (1 + \lambda K) - Y_{21} V_2 \sin(\theta_{21} - \delta) - Y_{22} V_2^2 \sin(\theta_{22}) = f_2(\delta, V_2, \lambda) \quad (3.10)$$

Now the original Jacobin matrix can be expressed as follows:

$$J_0 = \begin{bmatrix} \frac{\partial f_1}{\partial \delta} & \frac{\partial f_1}{\partial V_2} \\ \frac{\partial f_2}{\partial \delta} & \frac{\partial f_2}{\partial V_2} \end{bmatrix} = \begin{bmatrix} Y_{21} V_2 \sin(\theta_{21} - \delta) & Y_{21} \cos(\theta_{21} - \delta) + 2 Y_{22} V_2 \cos(\theta_{22}) \\ Y_{21} V_2 \cos(\theta_{21} - \delta) & -Y_{21} \sin(\theta_{21} - \delta) - 2 Y_{22} V_2 \sin(\theta_{22}) \end{bmatrix}$$

In the example, the system parameters are given as follows: $K = 1.0$, $P_0 = 0.1$, $\cos(\psi) = 1.0$, $Y_{12} = Y_{22} = 10$, $\theta_{12} = 90^\circ$, $\theta_{22} = -90^\circ$.

Suppose we start from the following initial point:

$$V_2 = 1.004, \quad \delta = 0.075^\circ, \quad \lambda = 0$$

Using the initial guess of V_2, a prediction of the next solution can be made by taking an appropriately sized step in a tangent direction to the solution path. The tangent vector can be calculated using the augmented Jacobin matrix:

$$J_{Aug} = \begin{bmatrix} J_0 & \frac{\partial f}{\partial \lambda} \\ e_k & \end{bmatrix} = \begin{bmatrix} \frac{\partial f_1}{\partial \delta} & \frac{\partial f_1}{\partial V_2} & P_0 * K \\ \frac{\partial f_2}{\partial \delta} & \frac{\partial f_2}{\partial V_2} & Q_0 * K \\ & e_k & \end{bmatrix} \quad (3.11)$$

where e_k is an appropriately dimensioned row rector with all elements equal to zero except the k^{th}, which equals one. If the index k is chosen correctly, the augmented matrix is nonsingular. In the beginning, $k = 3$ is chosen which corresponds to the parameter λ. So J_{Aug} is

$$J_{Aug} = \begin{bmatrix} 10.0392 & 0.13 & 0.1 \\ 0.1305 & 10.0808 & 0 \\ 0 & 0 & 1 \end{bmatrix}$$

Define the tangent vector as:

$$t = [d\delta \quad dV_2 \quad d\lambda]^T$$

During the prediction process, we have:

$$J_{Aug} * t = [0 \quad 0 \quad 1]^T \tag{3.12}$$

In the beginning the tangent vector is

$$t = [-0.01 \quad 0.0001 \quad 1]^T$$

With this tangent vector, we get the predicted solution:

$$\begin{bmatrix} \delta^{k+1} \\ V_2^{k+1} \\ \lambda^{k+1} \end{bmatrix} = \begin{bmatrix} \delta^k \\ V_2^k \\ \lambda^k \end{bmatrix} + \sigma \begin{bmatrix} d\delta^k \\ dV_2^k \\ d\lambda^k \end{bmatrix}$$

where σ is a specified step length (we start at an initial step length σ of 0.3. Subsequent step lengths can be determined according to the procedure described in Chapter 2). So we have

$$\begin{bmatrix} \overline{\delta}^1 \\ \overline{V}_2^1 \\ \overline{\lambda}^1 \end{bmatrix} = \begin{bmatrix} \delta^0 \\ V_2^0 \\ \lambda^0 \end{bmatrix} + \sigma \begin{bmatrix} d\delta^0 \\ dV_2^0 \\ d\lambda^0 \end{bmatrix} = \begin{bmatrix} 0.013 \\ 1.004 \\ 0 \end{bmatrix} + 0.3 * \begin{bmatrix} -0.01 \\ -0.0001 \\ 1 \end{bmatrix} = \begin{bmatrix} 0.01 \\ 1.004 \\ 0.3 \end{bmatrix}$$

Now that a prediction has been achieved, we can use this predicted solution as an initial guess for the corrector. We use the local parameterization method. Substituting these values into Eqs.3.9 and 3.10, we get the mismatch: $\Delta f_1^k, \Delta f_2^k$. Here we let λ^k be constant and apply the same augmented Jacobin matrix, to obtain the corrector:

$$\begin{bmatrix} \Delta\delta^{k+1} \\ \Delta V_2^{k+1} \\ \Delta\lambda^{k+1} \end{bmatrix} = -J_{Aug}^{-1} * \begin{bmatrix} \Delta f_1^k \\ \Delta f_2^k \\ 0 \end{bmatrix}$$

So the corrected solution is:

$$\begin{bmatrix} \delta^{k+1} \\ V_2^{k+1} \\ \lambda^{k+1} \end{bmatrix} = \begin{bmatrix} \delta^{k+1} \\ V_2^{k+1} \\ \lambda^{k+1} \end{bmatrix} + \sigma \begin{bmatrix} \Delta\delta^{k+1} \\ \Delta V_2^{k+1} \\ \Delta\lambda^{k+1} \end{bmatrix}$$

The final converged solution for a given tolerance (10^{-5}) is $[\delta^1 \quad V_2^1 \quad \lambda^1]^T = [-0.0129 \quad 1.0002 \quad 0.3]^T$. Then we can use this value as the starting point for the predictor and start the next step and so on.

After we get the tangent vector, we need to verify whether the system has reached the critical point. The sign of the product dVdλ provides the information related to the critical point ($d\lambda$=0 corresponds to the critical point. If the sign of the product dv$d\lambda$ is positive then the critical point has been passed).

The tracing process based on continuation method includes the following three situations:

a) Tracing the upper part of the PV curve
b) Tracing near the critical point
c) Tracing the lower part of the PV curve

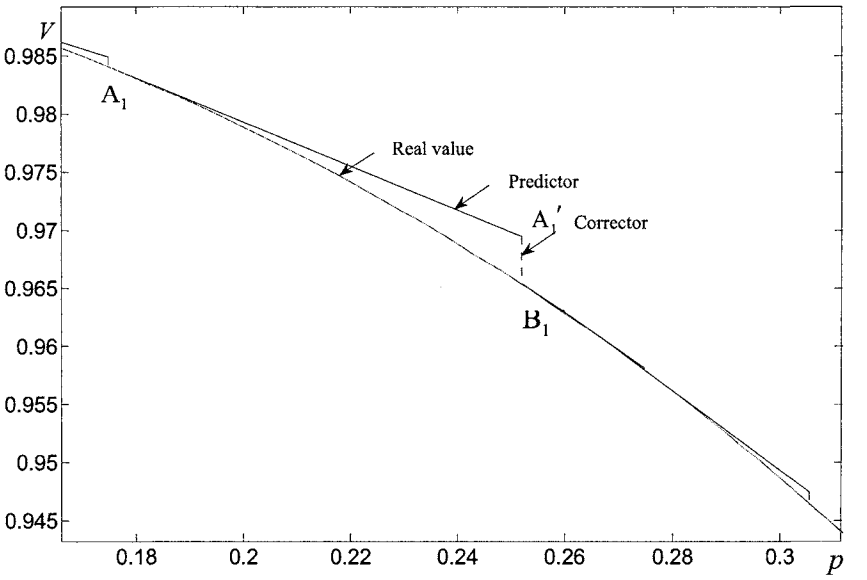

Fig.3.2 Tracing the upper part of the PV curve

a) Tracing the upper part of the PV curve:

As shown in Fig.3.2, suppose the predictor begins at A_1 (0.1750, 0.9841) ($p = PX/E^2$). At point A_1, the augmented Jacobian matrix is

$$J_{Aug} = \begin{bmatrix} 9.6837 & -1.7783 & 0.1 \\ -1.75 & 9.8406 & 0 \\ 0 & 0 & 1 \end{bmatrix}$$

So the tangent vector is

$$[d\delta \quad dV_2 \quad d\lambda]^T = [-0.0107 \quad -0.0019 \quad 1]^T$$

The estimated step length σ at this point is 7.68. Then the predictor becomes

$$\begin{bmatrix} \overline{\delta}^{k+1} \\ \overline{V}_2^{k+1} \\ \overline{\lambda}^{k+1} \end{bmatrix} = \begin{bmatrix} \delta^k \\ V_2^k \\ \lambda^k \end{bmatrix} + \sigma \begin{bmatrix} d\delta^k \\ dV_2^k \\ d\lambda^k \end{bmatrix} = \begin{bmatrix} -0.1788 \\ 0.9841 \\ 16.5 \end{bmatrix} + 7.68 * \begin{bmatrix} -0.0107 \\ -0.0019 \\ 1 \end{bmatrix} = \begin{bmatrix} -0.2608 \\ 0.9695 \\ 24.18 \end{bmatrix}$$

which corresponds to the point $A_1'(0.2518, 0.9695)$ in Fig.3.2. With same augmented Jacobian, one can perform corrector iterations using A_1' as initial guess for Newton method. After checking for proper convergence tolerance, the final solution is:

$$\begin{bmatrix} \delta^{k+1} \\ V_2^{k+1} \\ \lambda^{k+1} \end{bmatrix} = \begin{bmatrix} \overline{\delta}^{k+1} \\ \overline{V}_2^{k+1} \\ \overline{\lambda}^{k+1} \end{bmatrix} + \begin{bmatrix} \Delta\delta^{k+1} \\ \Delta V_2^{k+1} \\ \Delta\lambda^{k+1} \end{bmatrix} = \begin{bmatrix} -0.2639 \\ 0.9654 \\ 24.18 \end{bmatrix}$$

which is the point $B_1(0.2518, 0.9654)$. Then we can begin the next predictor.

b) Tracing near the critical point

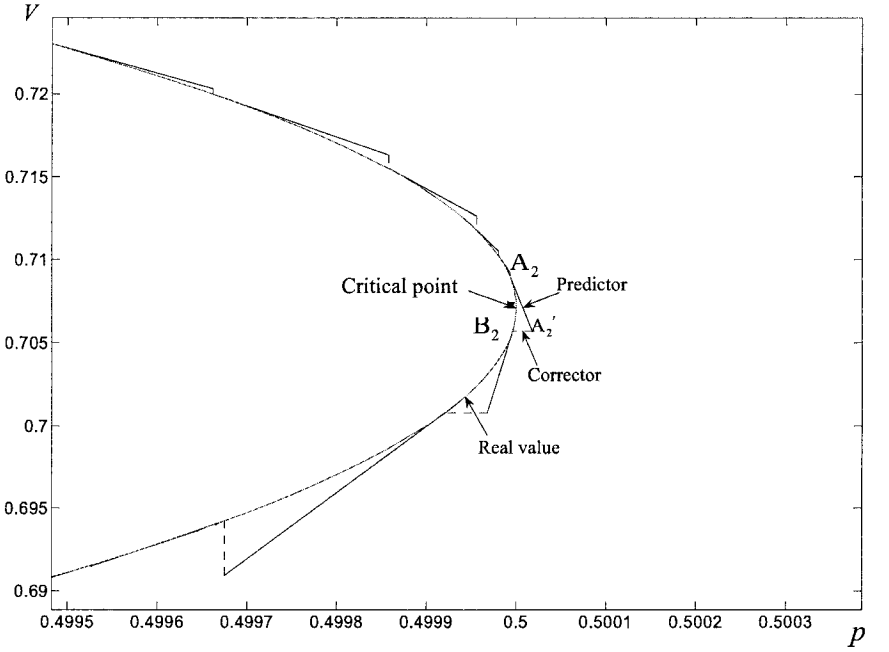

Fig. 3.3 Tracing near the critical point

As shown in Fig.3.3, suppose the predictor begins at $A_2(0.5, 0.709)$ which is close to the critical point. At point A_2, the augmented Jacobian matrix is

$$J_{Aug} = \begin{bmatrix} 5.0264 & -7.0524 & 0.1 \\ -4.9999 & 7.0897 & 0 \\ 0 & 0 & 1 \end{bmatrix}$$

So the tangent vector is

$$[d\delta \quad dV_2 \quad d\lambda]^T = [-1.893 \quad -1.335 \quad 1]^T$$

which corresponds to the point $A_2'(0.5, 0.7057)$ in Fig.3.3. It should be noted here that the absolute value of $d\lambda$ is less than the other tangent vector absolute values, so we changed the continuation parameter from λ to V_2 for the corrector. For the corrector convergence, the step length σ is reduced to 0.0025.

The final corrected solution:

$$\begin{bmatrix} \delta^{k+1} \\ V_2^{k+1} \\ \lambda^{k+1} \end{bmatrix} = \begin{bmatrix} \overline{\delta}^{k+1} \\ \overline{V}_2^{k+1} \\ \overline{\lambda}^{k+1} \end{bmatrix} + \begin{bmatrix} \Delta\delta^{k+1} \\ \Delta V_2^{k+1} \\ \Delta\lambda^{k+1} \end{bmatrix} = \begin{bmatrix} -0.7874 \\ 0.7057 \\ 48.9996 \end{bmatrix}$$

which is the point $B_2(0.5, 0.7057)$.

Actually the real critical point of the system is (0.5, 0.7071), which is very close to B_2.

c) Tracing below the critical point

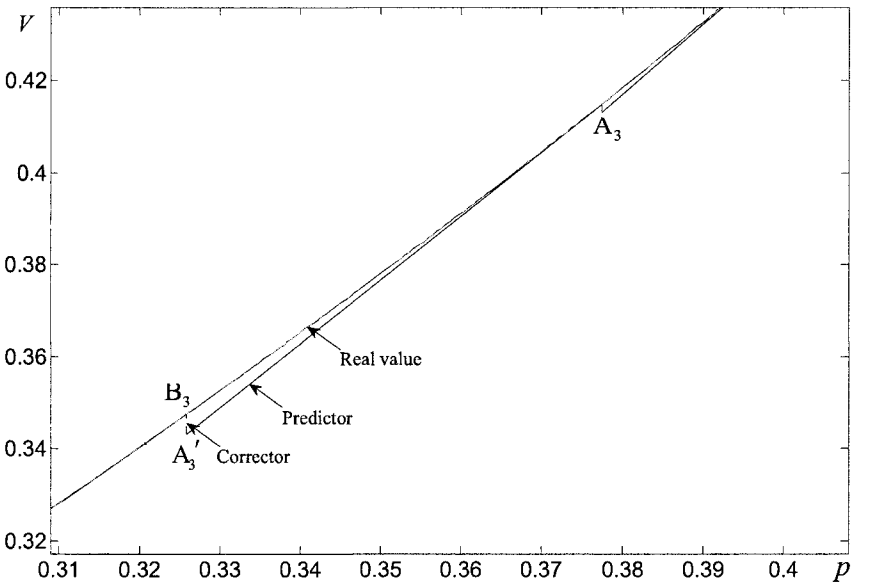

Fig. 3.4 Tracing below the critical

In Fig.3.4, suppose the predictor begins at A_3 (0.3774, 0.4147). At point A_3, the augmented Jacobian matrix is

$$J_{Aug} = \begin{bmatrix} 1.72 & -9.0995 & 0.1 \\ -3.7738 & 4.1473 & 0 \\ 0 & 0 & 1 \end{bmatrix}$$

So the tangent vector is

$$[d\delta \quad dV_2 \quad d\lambda]^T = [-0.0152 \quad -0.0139 \quad -1]^T$$

The predictor then becomes ($\sigma = 5.154$)

$$\begin{bmatrix} \overline{\delta}^{k+1} \\ \overline{V}_2^{k+1} \\ \overline{\lambda}^{k+1} \end{bmatrix} = \begin{bmatrix} \delta^k \\ V_2^k \\ \lambda^k \end{bmatrix} + \sigma \begin{bmatrix} d\delta^k \\ dV_2^k \\ d\lambda^k \end{bmatrix} = \begin{bmatrix} -1.1432 \\ 0.4147 \\ 36.7379 \end{bmatrix} + 5.154 * \begin{bmatrix} -0.0152 \\ -0.0139 \\ -1 \end{bmatrix} = \begin{bmatrix} -1.2217 \\ 0.3432 \\ 31.5839 \end{bmatrix}$$

which to the point A_3' (0.3258, 0.3432) in Fig.3.4. With same augmented Jacobian, one can perform corrector iterations using A_3' as initial guess for Newton method. After checking for proper convergence tolerance, the final solution is:

$$\begin{bmatrix} \delta^{k+1} \\ V_2^{k+1} \\ \lambda^{k+1} \end{bmatrix} = \begin{bmatrix} \overline{\delta}^{k+1} \\ \overline{V}_2^{k+1} \\ \overline{\lambda}^{k+1} \end{bmatrix} + \begin{bmatrix} \Delta\delta^{k+1} \\ \Delta V_2^{k+1} \\ \Delta\lambda^{k+1} \end{bmatrix} = \begin{bmatrix} -1.2159 \\ 0.3475 \\ 31.5839 \end{bmatrix}$$

which is the point B_3 (0.3258, 0.3475). Then we can begin the next predictor.

Finally, the whole tracing trajectory is shown in Fig.3.5. Compared with the PV curve for the example in Chapter 1, we can see that the results are identical. The PV curve in Fig.3.5 corresponds to unity power factor case of Fig.1.6 in Chapter 1.

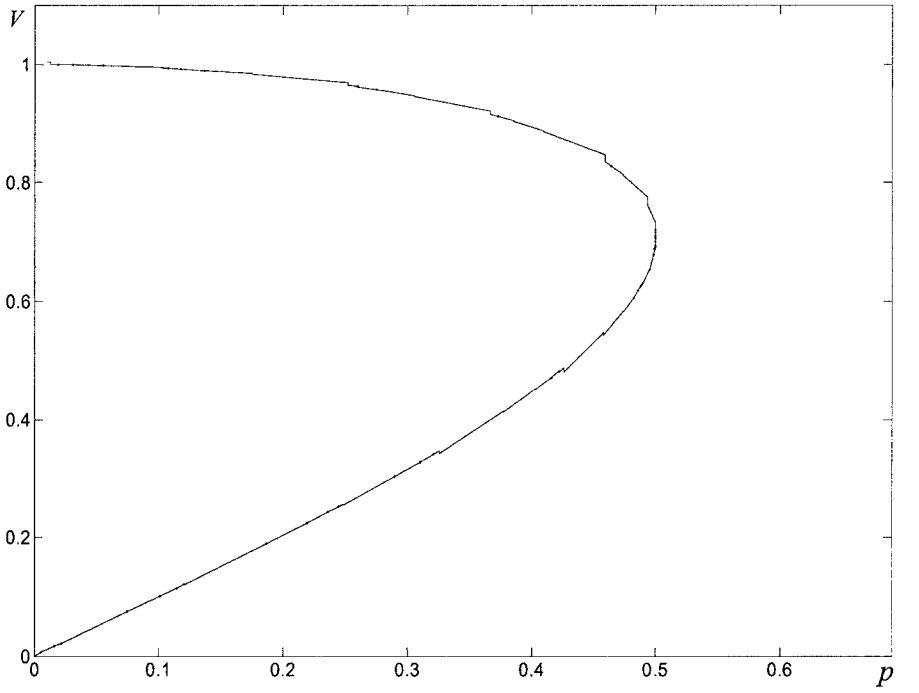

Fig. 3.5 The tracing trajectory

Two bus example: Nonlinear load:

The above two bus example is based on a constant power load model, and load is independent of voltage. Thus, load is made to vary in direct proportion to any change in λ. But in a nonlinear load model, the response of the load to a change in voltage magnitude must be considered, and in such load model, the load is not in direct proportion to change in λ. We can represent load increase scenario at bus 2 with nonlinear model as follows:

$$P = P_0(V_2 / V_{20})^{KPV} * (1 + \lambda K)$$
$$Q = Q_0(V_2 / V_{20})^{KQV} * (1 + \lambda K)$$

In the above equation, V_{20} is the initial voltage magnitude and parameter KPV and KPQ can be used to represent different load models. For example, $KPV = 0$, $KQV = 0$ is constant power model; $KPV = 1$, $KQV = 1$ is constant current model; $KPV = 2$, $KQV = 2$ is constant impedance model. With nonlinear load model, we can get new equations for real and reactive power:

$$0 = P_0(V_2 / V_{20})^{KPV} * (1 + \lambda K) + Y_{21}V_2 \cos(\theta_{21} - \delta) + Y_{22}V_2^2 \cos(\theta_{22}) = f_1(\delta, V_2, \lambda)$$

$$0 = Q_0(V_2 / V_{20})^{KQV} * (1 + \lambda K) - Y_{21}V_2 \sin(\theta_{21} - \delta) - Y_{22}V_2^2 \sin(\theta_{22}) = f_2(\delta, V_2, \lambda)$$

We use constant current and constant impedance load model to demonstrate the effect of different load model on critical point with 2 bus system. In the simulation, the system parameters are given as follows: $K = 1.0$, $P_0 = 0.14$, $\cos\psi = 1.0$, $Y_{12} = Y_{22} = 10$, $\theta_{12} = 90°$, $\theta_{22} = -90°$.

Figs 3.6, 3.7 and 3.8 show PV curve, P-λ, and V-λ for constant current load model. As parameter λ increases, power consumption first increases and reaches maximum and then decreases. Here λ_{max} does not correspond to P_{max}. Here λ can be interpreted as connected load as opposed to actual load.

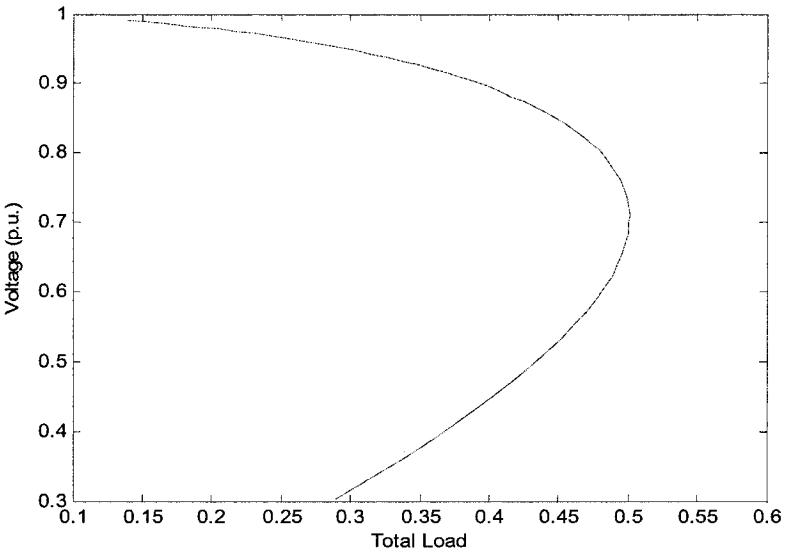

Fig. 3.6 V vs. P curve for constant current load

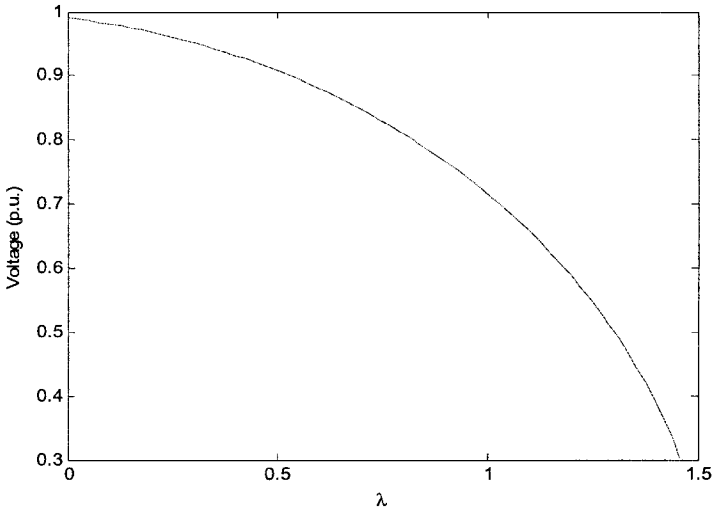

Fig. 3.7 V vs. λ curve for constant current load

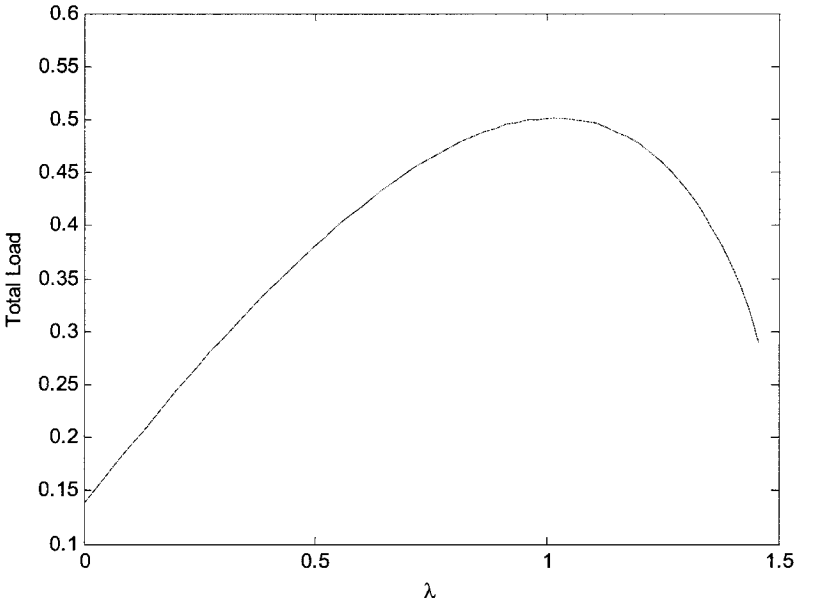

Fig. 3.8 P vs. λ for constant current load

Figs. 3.9, 3.10 and 3.11 show PV curve, P-λ, and V-λ for constant impedance load.

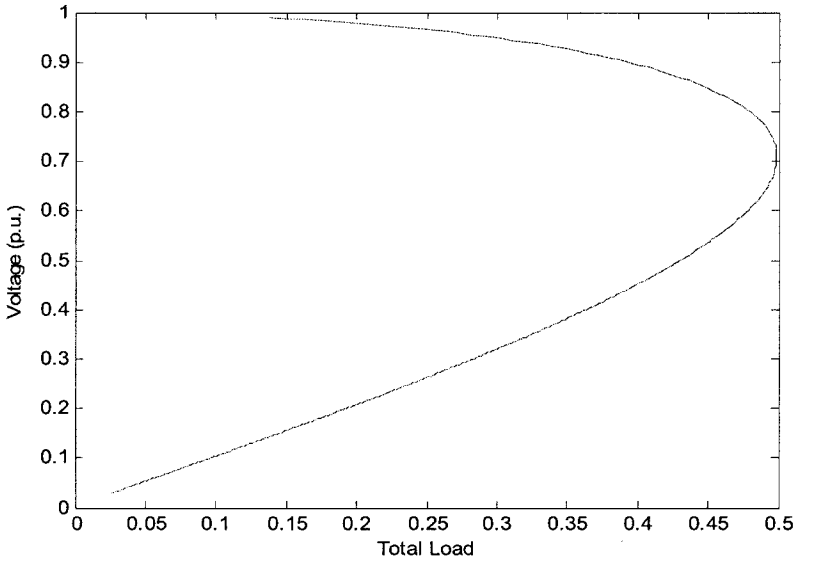

Fig. 3.9 V vs. P curve for constant impedance load

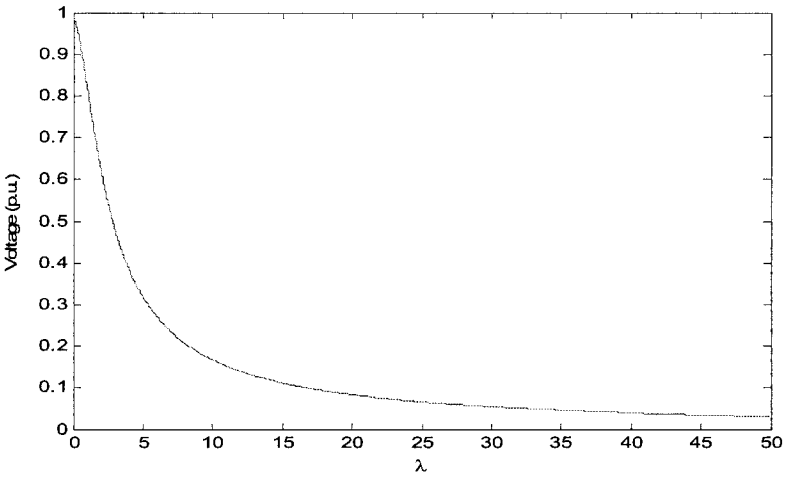

Fig. 3.10 V vs. λ curve for constant current load

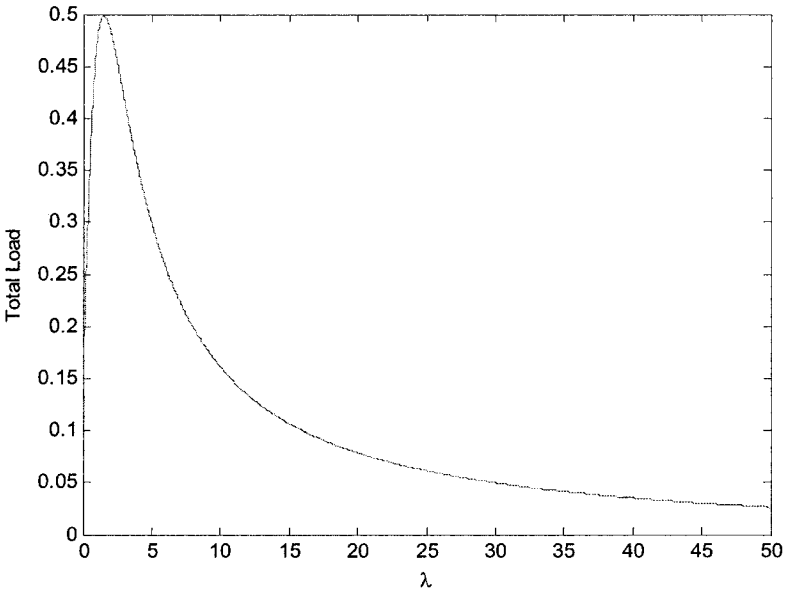

Fig. 3.11 P vs. λ for constant current load

For example if it is purely a resistive load then λ represents the number of parallel resistors connected at bus2. As we can see form the Fig. 3.11 , P_{max} occurs when the reactance of the transmission line(here we neglected the resistance of the transmission line) equals the total resistance connected at bus2. As the number of resistors increase beyond the one correspond to the maximum power, net load power decreases. The voltage at bus 2 also decreases with λ as shown in Fig. 3.10.

39 bus New England test system example

The data related to this test system is given in Appendix A: three scenarios are considered to demonstrate the capability of the continuation power flow.

Scenario 1

In the scenario 1, loads at 8 buses are increased, while the increased load is picked up by 9 generators. These load buses are bus 7, 8, 15, 16, 18, 20, 21, 23, and the load is increased proportional to their initial load levels. Scheduled generator buses are generators 30, 31, 32, 33, 34, 35, 36, 37, 38. The generator output is also increased proportional to their initial generations. Among these 9 generators, generator 31 is chosen as the slack bus. Besides scheduled generation output increment, generator 31 is also responsible for the load balance of the network.

For the load, the load increment is defined as:

$$P_{Li}(\lambda) = P_{Li0}[1 + \lambda K_{Li}]$$
$$Q_{Li}(\lambda) = P_{Li0}\tan(\Psi i)[1 + \lambda K_{Li}]$$
$$K_{Li} = P_{Total} / \sum P_{Li0}$$

The initial total load (P_{Total0}) is 6141MW with $\lambda = 0$, and in the next step, the total load is 6783MW with $\lambda = (6783 - 6141)/6141 = 0.104548$. The total load increment is 642MW which is distributed among 8 load buses proportional to their initial bus load. The following Table 3.1 shows the initial bus load level, the coefficients K_L , bus load increment, new load level and the power factor at each bus:

Table 3.1 Scenario 1 for load variation

Bus	Initial Load (MW)	K	Load Increment (MW)	New Load Level (MW)	Power Factor
7	233.8	2.221326	54.15286	287.9529	0.94 Lagging
8	522	2.221326	120.9059	642.9059	0.95 Lagging
15	320	2.221326	74.11854	394.1185	0.90 Lagging
16	329.4	2.221326	76.29577	405.6958	0.93 Lagging
18	158	2.221326	36.59603	194.596	0.98 Lagging
20	680	2.221326	157.5019	837.5019	0.99 Lagging
21	274	2.221326	63.464	337.464	0.92 Lagging
23	247.5	2.221326	57.32606	304.8261	0.95 Lagging

For the generator

$$P_{Gi} = P_{Gi0}(1 + \lambda K_{Gi})$$
$$K_{Gi} = P_{Gi0} / \sum P_{Gi0}$$

The following Table 3.2 shows the initial generator output, the coefficients K_G, generation increment and new generation level:

Table 3.2 Scenario 1 for generation distribution

Generators	Initial Generation (MW)	K_G	Generation Increment (MW)	New Generation (MW)
30	230	1.185	28.41914	258.4191
31	722.53	1.185	89.27687	811.8069
32	630	1.185	77.84372	707.8437
33	612	1.185	75.61962	687.6196
34	488	1.185	60.29799	548.298
35	630	1.185	77.84372	707.8437
36	540	1.185	66.72319	606.7232
37	520	1.185	64.25196	584.252
38	810	1.185	100.0848	910.0848

Because generator 31 is the slack bus, the actual output is 827MW instead of scheduled 811MW, and the additional 16MW is for the load balance.

Fig.3.12 shows the variation of individual generators real power with total system load. Fig.3.13 shows the variation of individual bus load with respect to the total system load. Fig.3.14 presents PV curves at four critical load buses (these buses are based on the largest tangent vector elements corresponding to voltages at the critical point). Fig.3.15 shows the relationship between the bus voltage and the parameter λ. For constant power loads $\lambda_{\max}$ corresponds to $P_{\max}$. However for nonlinear loads $\lambda_{\max}$ does not correspond to $P_{\max}$ as shown in two bus example.

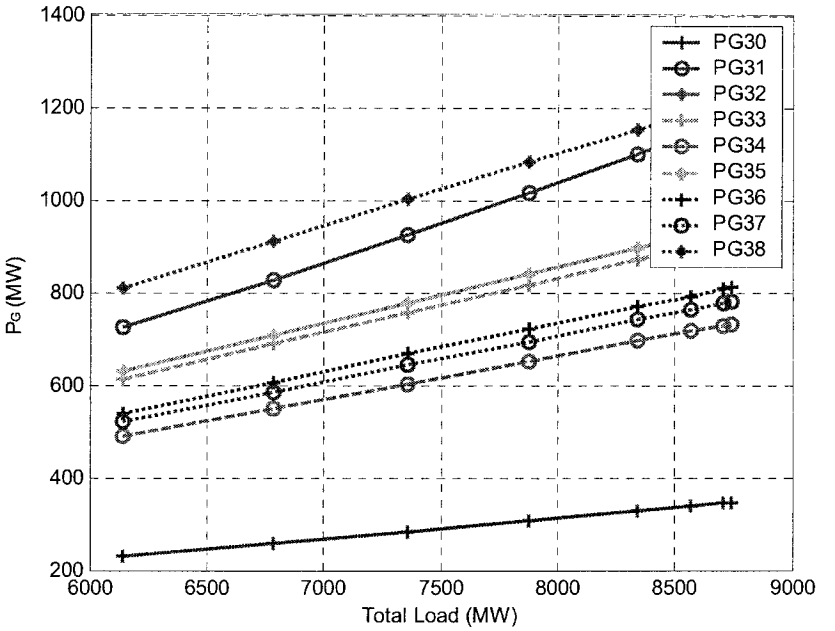

Fig.3.12 P_G vs. P_{total}

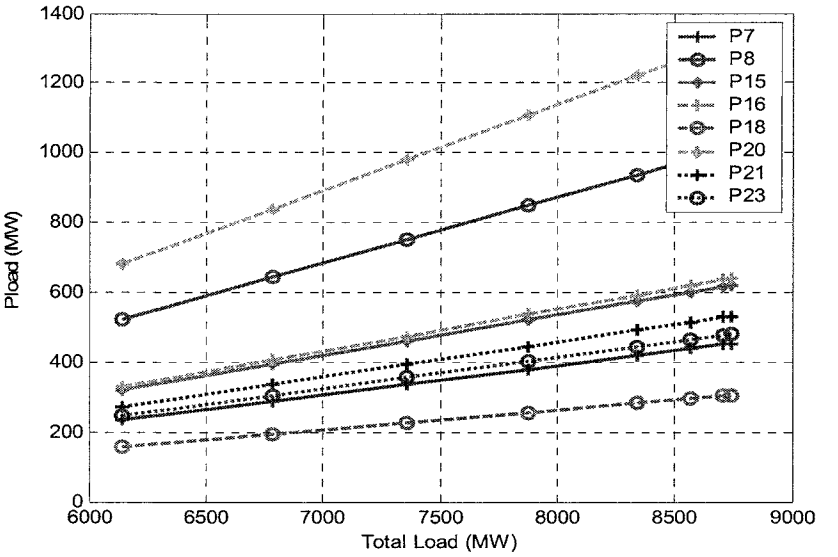

Fig.3.13 P_{load} at bus vs. P_{total}

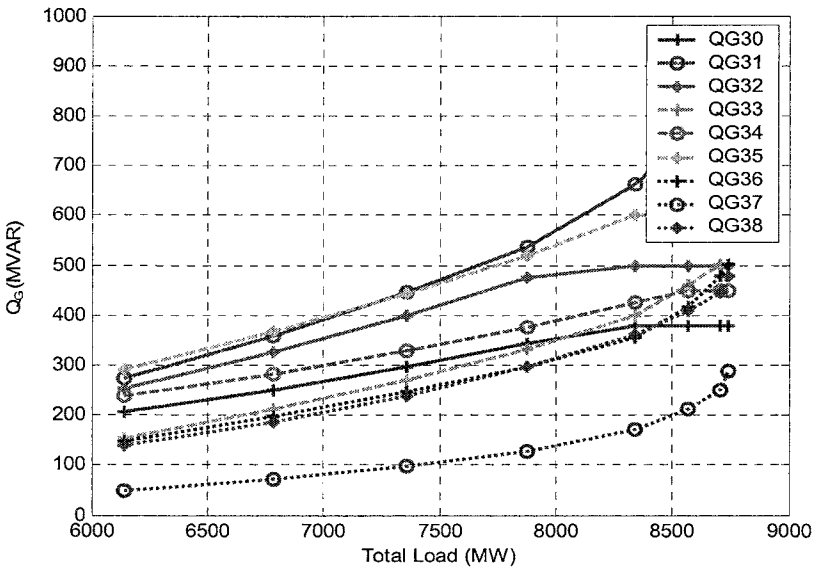

Fig.3.14. Q_g vs. P_{total}

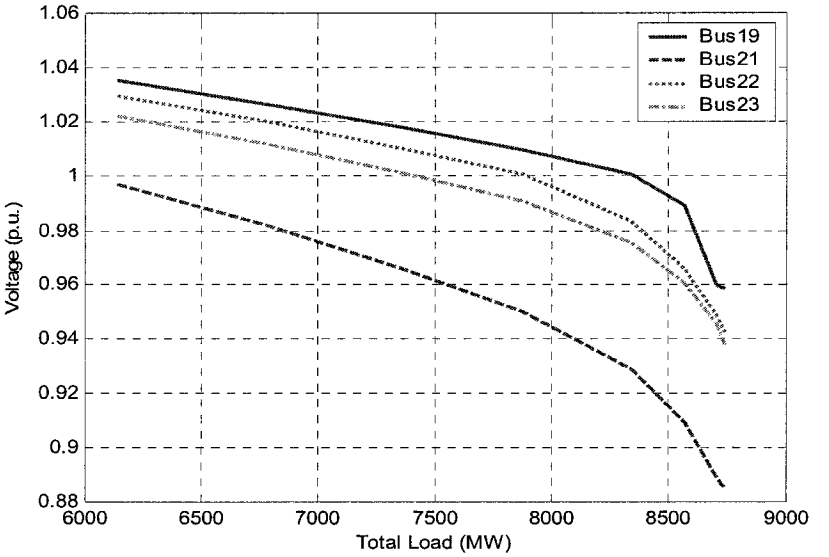

Fig.3.15 V vs. P_{total}

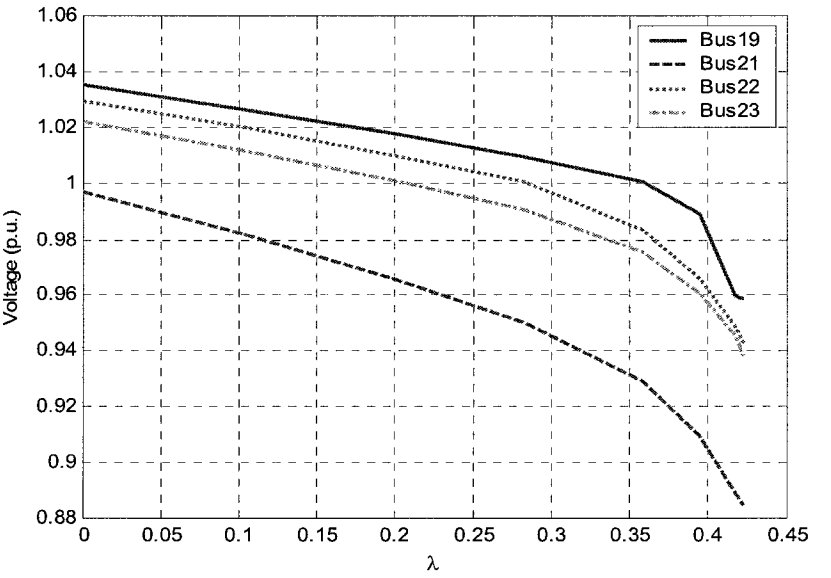

Fig.3.16 V vs. λ

Scenario 2

The only difference in this scenario compared to scenario 1 is that the loads at those 8 buses are increased equally. This means load increment is the same among all the load buses. All other conditions are same as in scenario1.

Table 3.3 Scenario 2 for load variation

Bus	Initial Load (MW)	K	Load Increment (MW)	New Load Level (MW)
7	233.8	3.283136	79.16	312.96
8	522	1.470493	79.17	601.17
15	320	2.398741	79.16	399.16
16	329.4	2.330289	79.17	408.57
18	158	4.85821	79.16	237.16
20	680	1.128819	79.18	759.18
21	274	2.80145	79.17	353.17
23	247.5	3.101403	79.15	326.65

Figs.3.17 to 3.21 are similar to Fig.3.12 to 3.16 respectively.

The initial total load is 6141MW with $\lambda = 0$, and in the next step, the total load is 6774MW with $\lambda = (6774 - 6141)/6141 = 0.103127$. The total load increment is 633MW which is distributed among 8 load buses equally. The following Table 3.3 shows the initial bus load level, the coefficients K_L, bus load increment and new bus load level. The power factor at each bus is same as in scenario1.

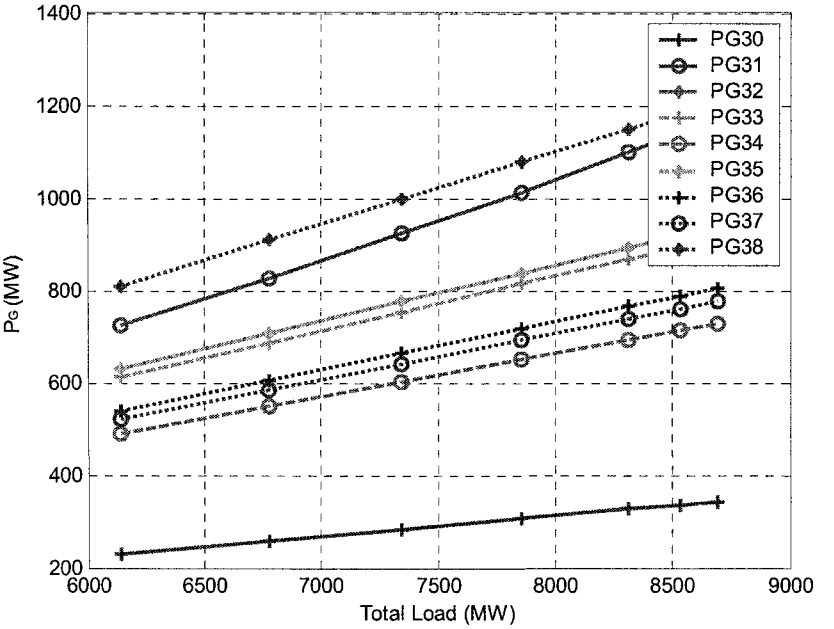

Fig.3.17 P_g vs. P_{total}

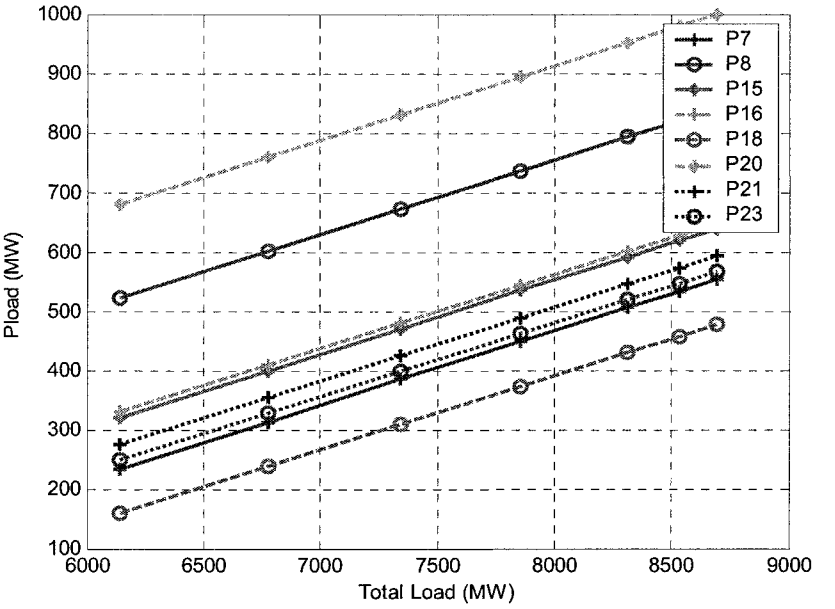

Fig 3.18 P_{load} at various buses vs. P_{total}

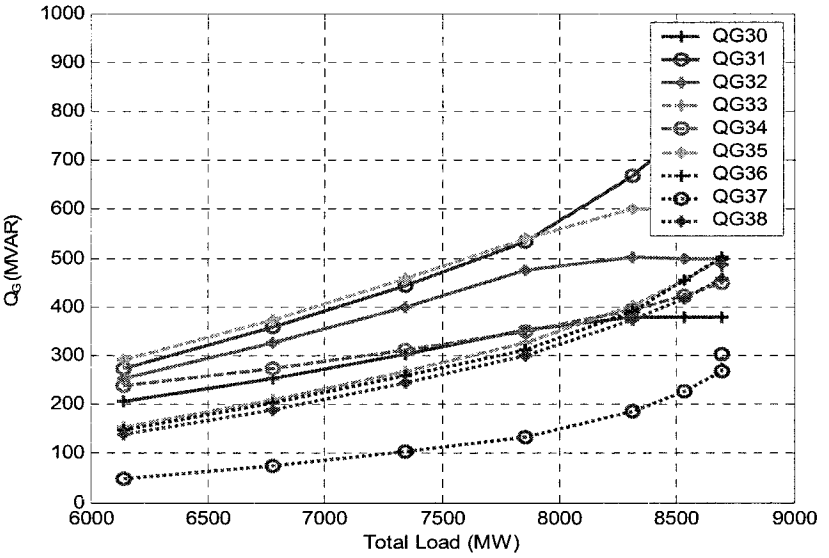

Fig. 3.19 Q_G vs. P_{total}

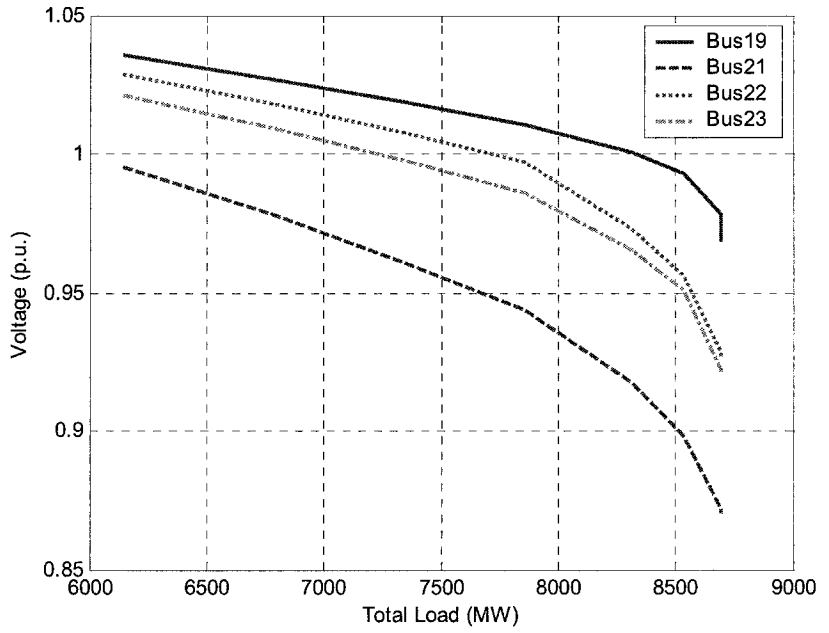

Fig.3.20 V vs. P_{total}

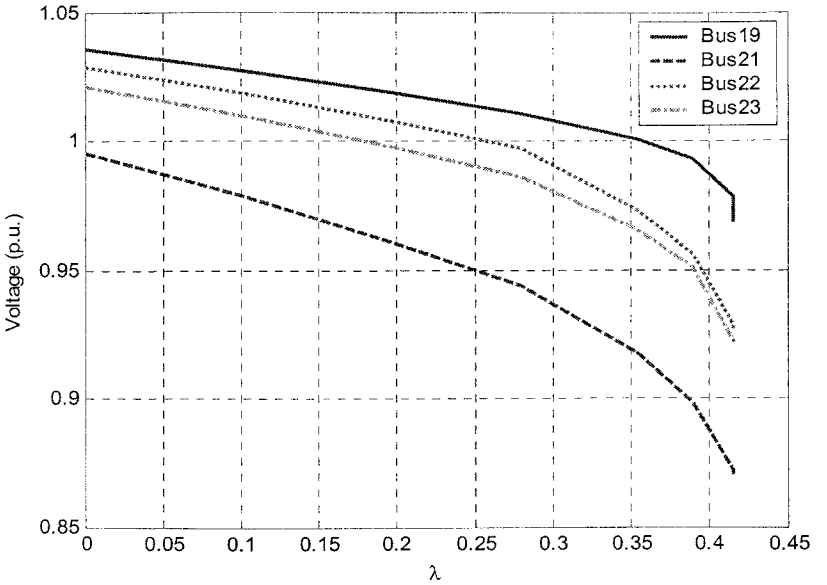

Fig 3.21 V vs. λ

3.6 Simultaneous Equilibria Tracing in Power Systems

In power system analysis, it is frequently of interest to find solutions of the system at an equilibrium point. For instance, the solution of the power flow equations is needed in system planning and static security analysis. In stability analysis, a power flow is used to calculate the voltages and angles at all buses, and then the dynamic state variables are evaluated using the device equations. This procedure causes some problems as will be shown in the following sections. To overcome these problems, we will further extend the continuation technique to simultaneously trace the total system equlibria of the structure preserving power system model, which is described by a set of nonlinear differential and algebraic equations (DAEs). Physical interpretations of the new approach will give insights into some issues which are important to a good understanding of the power system.

Unlike in power flow analysis, a detailed dynamic representation of the power system is required to analyze the system's stability behavior. As a typical nonlinear dynamic system, with the multiple time-scale property, a set of nonlinear DAEs can be employed to describe the behavior of the power system, i.e.,

$$\dot{X} = F(X,Y,P) \tag{3.13}$$

$$0 = G(X,Y,P) \tag{3.14}$$

where X includes the dynamic states, Y includes the algebraic state variables, and P consists of all parameters explicitly appearing in F and G. Some of these parameters can be control input settings.

3.6.1 Total solution at an equilibrium

A system equilibrium solution is needed for the evaluation of the stability, the solution X_0 and Y_0 of Eqs.3.13 and 3.14 at steady state, i.e., when $\dot{X} = 0$, constitute the equilibrium point. Setting the differential to zero indicates a state of equilibrium of the system. In small signal stability analysis, the right hand side of the DAEs is first linearized, and then the system state matrix A_{sys} (where $A_{sys} = F_X - F_Y G_Y^{-1} G_X$, see section 3.8.7) is evaluated at (X_0, Y_0). Its eigenvalues give small signal stability information of the current equilibrium point. In nonlinear time domain analysis, the equilibrium solution (X_0, Y_0) gives the initial conditions to start numerical integration. In direct Lyapunov type stability analysis, this solution is also required.

3.6.2 Traditional approach

In Eq.3.14, G corresponds to the power balance equations at all buses in the system. Therefore its dimension is larger than that of the power flow. In power flow, it is assumed that the voltage at PV buses and voltage and angle at the slack bus(es) are known and constant. Consequently, for a network of n buses, if there are m generators, m_s of which are designated as slack, then the number of equations in the power flow formulation will be $2n - m - m_s$ (for polar coordinates). For a constant generator terminal voltage, it is assumed that the static gain of the excitation system is infinite. No limitations on the slack bus generation can be enforced during the solution process. Once a power flow is solved, together with the pre-specified generation and voltages for PV and slack buses, the X_0

values will be updated using Eq.3.13 at steady state. The control parameter settings in P corresponding to this X_0 are then computed. This procedure of solving for (X_0, Y_0, P_0) is termed as the two-step approach. With this total system equilibrium solution, further stability analysis can then be conducted.

The above procedure has some drawbacks. Firstly, if control limits are enforced, a solution (X_0, Y_0, P_0) satisfying these limits may not exist. The slack bus generation might also exceed limits after the power flow. In this case, the state which is limited would need to be fixed at its limiting value and a corresponding new steady state equilibrium solution would have to be found. This would require a new power flow, for each specified value of PV bus generation or terminal voltage, or possibly generator reactive power injection. For the last case, the generator voltage becomes part of the power flow solution. For a heavily loaded system, this trial and error procedure may have to be repeated several times, each time requiring a new power flow solution. Secondly, even after a set of (X_0, Y_0, P_0) values satisfying all limits are found, there still exists another problem which is inevitable in using the power flow based two-step approach to produce equilibria solution for stability analysis. That is, the description of the generators in the power flow is very different from that in the dynamic response. How the generators behave in a dynamic process depends on the dynamic characteristics of the synchronous machine and the control systems associated with them. These controls are not represented for the PV bus generators and the slack bus generators are simply left out in the power flow. Therefore, it may not be unusual that this discrepancy in representation leads to erroneous results.

3.7 Power Flow Methodology and Assumptions

Before introducing the simultaneous equilibria tracing technique, let us first have a closer look at the assumptions used in the power flow, particularly the reasons why they are needed. With a clearer understanding of these assumptions, we will then be able to devise a procedure in which the problems encountered in the traditional approach can be avoided.

3.7.1 Nonlinearity in power flow

In normal electrical network analysis, the voltages and/or currents of power sources are given as known quantities. In order to find the voltages at various nodes and currents in all branches, one simply needs to solve the network nodal equations which are linear. Correspondingly, for power network, this refers to the nodal representation, given in phasor notation as

$$Y\overline{V} = \overline{I} \tag{3.15}$$

where Y is the network admittance matrix, $\overline{V}$ is the vector of phasor voltages at all buses, and $\overline{I}$ is the nodal phasor injection currents. The conditions for Eq.3.15 to have a solution with a specified set of injection currents $\overline{I}$ are

- Y is nonsingular;
- $\text{rank}(Y \mid \overline{I}) = \text{rank}(Y)$ if Y is singular.

Were the injection currents known, the power flow would have involved no nonlinear equations. However, in power system analysis, the nodal voltages and injection currents are both unknown before a power flow is solved. Instead, the generation and load powers are given as the known quantities. They are related to the nodal voltages and injection currents as shown below.

$$\begin{aligned}\overline{I_i} &= \frac{S_{Gi} - S_{Li}}{\overline{V_i}^*} \\ &= \frac{(P_{Gi} - P_{Li}) + j(Q_{Gi} - Q_{Li})}{\overline{V_i}^*}\end{aligned}$$

The '*' sign indicates the complex conjugate. With the real and imaginary parts separated, Eq.3.15 is transformed into the following form

$$0 = P_{Ei} - P_{Li} - P_{Ti} \qquad i = 1, \cdots n \tag{3.16}$$

$$0 = Q_{Ei} - Q_{Li} - Q_{Ti} \qquad i = 1, \cdots n \tag{3.17}$$

where

$$P_{Ti} = V_i \sum_{k=1}^{n} V_k y_{ik} \cos(\theta_i - \theta_k - \gamma_{ik}) \tag{3.18}$$

$$Q_{Ti} = V_i \sum_{k=1}^{n} V_k y_{ik} \sin(\theta_i - \theta_k - \gamma_{ik}) \tag{3.19}$$

The two nonlinear Eqs.3.16 and 3.17 correspond to the algebraic part of the DAE formulation given in Eq.3.14. With the powers specified at the terminal buses, X variables are not of concern in the power flow equations.

3.7.2 Slack bus assumption

The unknowns in Eqs.3.16 and 3.17 are $(\underline{V}, \underline{\theta})$, the number of which is $2n$. The underline sign is used to denote vectors. If we want o solve these unknowns directly using the Newton's method, we have to specify the generations and load powers at all buses. And most probably, with a starting point $(\underline{V}^0, \underline{\theta}^0)$ close to normal operating conditions, this approach will lead to divergence. A closer look of the structure of the power balance equations will give more insight into the problem. Designating the generator at the n^{th} bus as the slack, summing up the first $n-1$ equations in Eqs.3.16 and 3.17 and then adding them to the n^{th} and $2n^{th}$ equations respectively will yield

$$P_{Gs} = \sum_{i=1}^{n} P_{Li} + P_{loss}(\underline{V}, \underline{\theta}) - \sum_{i=1}^{n-1} P_{Ei} \tag{3.20}$$

$$Q_{Gs} = \sum_{i=1}^{n} Q_{Li} + Q_{loss}(\underline{V}, \underline{\theta}) - \sum_{i=1}^{n-1} Q_{Ei} \tag{3.21}$$

Since we know that

$$\sum_{i=1}^{n} P_{Ti} = P_{loss}(\underline{V}, \underline{\theta})$$

$$\sum_{i=1}^{n} Q_{Ti} = Q_{loss}(\underline{V}, \underline{\theta})$$

These two equations can be put together with the first $n-1$ equations from 3.16 and 3.17 respectively to represent the complete network. Eqs. 3.20 and 3.21 show that, if a solution $(\underline{V}^*, \underline{\theta}^*)$ exists, for a possible successful convergence, we must specify the generations subject to the constraints given in Eqs.3.20 and 3.21. Since the losses as a function of the network solution are unknown before the power flow is solved, it is practically impossible to do so. Therefore, it is very likely that, if we have to specify the power generations for all generators, constraints Eqs.3.20 and 3.21 may be greatly violated, and correspondingly the staring point $(\underline{V}^0, \underline{\theta}^0)$ might be well out of the radius of convergence of the Newton's method. Also, there is a possibility that a *real* solution simply does not exist corresponding to this set of specified generations. (From algebraic equations theory, we know that a solution always exists if we also consider complex roots.) If one can devise a scheme so that there is freedom of adjusting the generation during the course of iteratively solving the power flow equations, then convergence performance might be much better. Referring to this, an immediate thought would be to eliminate Eqs.3.20 and 3.21 altogether from the power flow iterations. Consequently, the slack bus generation need not be specified. To do so, we must remove two unknowns from $(\underline{V}, \underline{\theta})$. This is no difficulty at all. Because the goal of a power flow is to give a dispatch of the generation so that the system load can be served with the bus voltages being close to normal operating conditions, usually close to 1.0 p.u., we can reasonably assign 1.0 to V_s and 0^0 to θ_s, the latter of which is simply to set a reference for the angle measurement, and thus it is arbitrary. After the power flow converges, we then calculate the losses and assign all of them to the slack generators. This procedure makes sure that the loss-generation imbalance does not cause convergence trouble during iteration. And this imbalance is fixed *only* after the power flow is solved. The above discussion shows that the slack bus assumption is a mathematical requirement for possible/good convergence of the Newton's iterative algorithm.

3.7.3 PV bus assumption

In order to maintain the system voltage levels, the generators are equipped with automatic voltage regulators (AVR) so that terminal voltages are within limits during system load increase or other disturbances. With the power flow description of the system, the only way to reflect this fact is to force the terminal voltages at the generator buses as constant since AVR is

not represented. To achieve this, the reactive power balance equations for generator buses must be removed. As a consequence, Q_{Ei} is no longer needs to be specified as input, it is released as a variable. Physically, this means that reactive support from generators helps maintain a relatively high and steady terminal voltage. Numerically, this possibly also leads to better convergence characteristics of the Newton-Raphson power flow algorithm.

After the above discussion, we are now ready to devise a strategy that eliminates the unreasonable assumptions used in the power flow. It solves for a reasonable set of (X,Y) values with control limits automatically implemented. This leads us to the topic of simultaneous equilibria tracing technique.

3.8 Total Power System Equilibria Solutions

From the discussion given in Section 3.7 , we can make two conclusions about the assumptions used in the power flow:

- *Slack bus methodology* provides a means of "automatically" adjusting real and reactive power generation "during" the iteration, not at all buses, but only for the slack, so that at any iteration the losses are not causing the point to be too far away from the true solution, therefore making Newton's iterative method possible to converge.
- *The PV bus assumption* is used to reflect the need of maintaining the system voltage levels by AVRs and it also possibly helps improve the convergence rate of the Newton-Raphson algorithm.

In the following sections, we will study how these assumptions, which cause the problems mentioned in subsection 3.6.2 can be removed, while the goals they are made to achieve are not sacrificed.

Before we introduce the simultaneous equilibria tracing technique, let us first give a detailed representation of the structure-preserving power system model.

3.8.1 Formulation of power system DAE model

A power system is assumed to have n buses and m generators. Each generator is assumed to be equipped with the same type of excitation control system and speed governor. The formulation of power system modeling is presented in this chapter. The commonly used power system notations are adopted here.

3.8.1.1 Synchronous generators

Without loss of generality, the rotor angle of the m^{th} generator is chosen as the system angle reference. This choice of reference is different from the conventional slack bus selection. No assumptions are necessary for choosing such a reference. When stator transients are ignored, the two-axis model [5, 6] describing the synchronous machine dynamics can be given as:

$$\dot{\delta}_i = (\omega_i - \omega_{\mathrm{m}})\omega_0 \qquad i = 1, \cdots, m-1 \tag{3.22}$$

$$\begin{aligned} \dot{\omega}_i = M_i^{-1}[& P_{mi} - D_i(\omega_i - \omega_m) - (E'_{qi} - X'_{di} I_{di}) I_{qi} \\ & - (E'_{di} + X'_{qi} I_{qi}) I_{di}] \quad i = 1, \cdots, m \end{aligned} \tag{3.23}$$

$$\dot{E}'_{qi} = T_{d0i}^{-1}[E_{fdi} - E'_{qi} - (X_{di} - X'_{di}) I_{di}] \quad i = 1, \cdots, m \tag{3.24}$$

$$\dot{E}'_{di} = T_{q0i}^{-1}[-E'_{di} + (X_{qi} - X'_{qi}) I_{qi}] \quad i = 1, \cdots, m \tag{3.25}$$

where ω_m is the system frequency, ω_i is the machine frequency, namely, generator angular speed and ω_0 is the system rated frequency (377.0 *rad /sec*). I_{di} and I_{qi} are direct axis and quadrature axis currents respectively; E'_{di} and E'_{qi} are transient direct axis and quadrature axis EMF respectively; T_{d0i} and T_{q0i} are direct axis and quadrature axis open circuit time constants respectively; X'_{di} and X'_{qi} are direct axis and quadrature axis transient reactances and R_{si} are armature resistance of

the machine; M_i is inertia constant and D_i is the damping constant of the machine. All the quantities are in per unit except ω_0.

Interface voltage equations to the network are given as follows:

$$E'_{qi} = V_i \cos(\delta_i - \theta_i) + R_{si} I_{qi} + X'_{di} I_{di} \tag{3.26}$$

$$E'_{di} = V_i \sin(\delta_i - \theta_i) + R_{si} I_{di} - X'_{qi} I_{qi} \tag{3.27}$$

where V_i and θ_i are bus voltage and angle respectively.

The machine currents I_{di} and I_{qi} can be eliminated by solving the generator interface equations to the network. Hence,

$$I_{di} = [R_{si} E'_{di} + E'_{qi} X'_{qi} - R_{si} V_i \sin(\delta_i - \theta_i) - X'_{qi} V_i \cos(\delta_i - \theta_i)] A_i^{-1} \tag{3.28}$$

$$I_{qi} = [R_{si} E'_{qi} - E'_{di} X'_{di} - R_{si} V_i \cos(\delta_i - \theta_i) - X'_{di} V_i \sin(\delta_i - \theta_i)] A_i^{-1} \tag{3.29}$$

$$A_i = R_{si}^2 + X'_{di} X'_{qi} \tag{3.30}$$

Note that Eq.3.22 does not include the differential equation for δ_m, and all the angles here and henceforth are relative angles with respect to the m^{th} generator's rotor angle.

3.8.1.2 Excitation Control system

The simplified IEEE type DC-1 excitation system [5] as shown in Fig.3.22 is used here. The corresponding mathematical model is

$$\dot{E}_{fdi} = T_{ei}^{-1} [V_{ri} - [S_{ei}(E_{fdi})] E_{fdi}] \quad i = 1, \cdots, m \tag{3.31}$$

$$\dot{V}_{ri} = T_{ai}^{-1} [-V_{ri} + K_{ai}(V_{refi} - V_i - R_{fi})] \quad i = 1, \cdots, m \tag{3.32}$$

If $V_{ri,\min} \le V_{ri} \le V_{ri,\max}$, $V_{pssi} = 0$ (at steady state),

$$\dot{R}_{fi} = T_{fi}^{-1}[-R_{fi} - [K_{ei} + S_{ei}(E_{fdi})]K_{fi}E_{fdi} / T_{ei} + K_{fi}V_{ri} / T_{ei} \quad (3.33)$$

where V_{ref} is the reference voltage of the automatic voltage regulator (AVR); V_{ri} and R_{fi} are the outputs of the AVR and exciter soft feedback; E_{fdi} is the voltage applied to generator field winding; T_{ai}, T_{ei} and T_{fi} are AVR, exciter and feedback time constants respectively ; K_{ai}, K_{ei} and K_{fi} are gains of AVR, exciter and feedback respectively; $V_{ri,\min}$ and $V_{ri,\max}$ are the lower and upper limits of V_{ri} respectively.

3.8.1.3 Prime mover and speed governor

Fig.3.23 shows the block diagram for a simplified prime mover and speed governor. Two differential equations are involved to describe the dynamics when no μ_i limit is hit.

$$\dot{P}_{mi} = T_{chi}^{-1}(\mu_i - P_{mi}) \qquad i = 1, \cdots, m \quad (3.34)$$

$$\dot{\mu}_i = T_{gi}^{-1}[P_{gsi}(\omega_i - \omega_{ref}) / R_i - \mu_i] \qquad \text{if } \mu_{i,\min} \le \mu_i \le \mu_{i,\max} \quad i = 1, \cdots, m \quad (3.35)$$

where $P_{gsi} = P_{gsi}^0(1 + K_{gi}\mu)$ is the designated real power generation; P_{gsi}^0 is its setting at base case; K_{gi} is the generator load pick-up factor that could be determined by AGC, EDC or other system operating practice; P_{mi} is the mechanical power of prime mover and μ_i is the steam valve or water gate opening; R_i is the governor regulation constant representing its inherent speed-droop characteristic; ω_{ref} (=1.0) is the governor reference speed; T_{chi} and T_{gi} are the time constants related to the prime mover and speed governor respectively; $\mu_{i,\min}$ and $\mu_{i,\max}$ are the lower and upper limits of μ, where a parameter μ is introduced to designate the system operation scenario. At the base case, μ equals to zero.

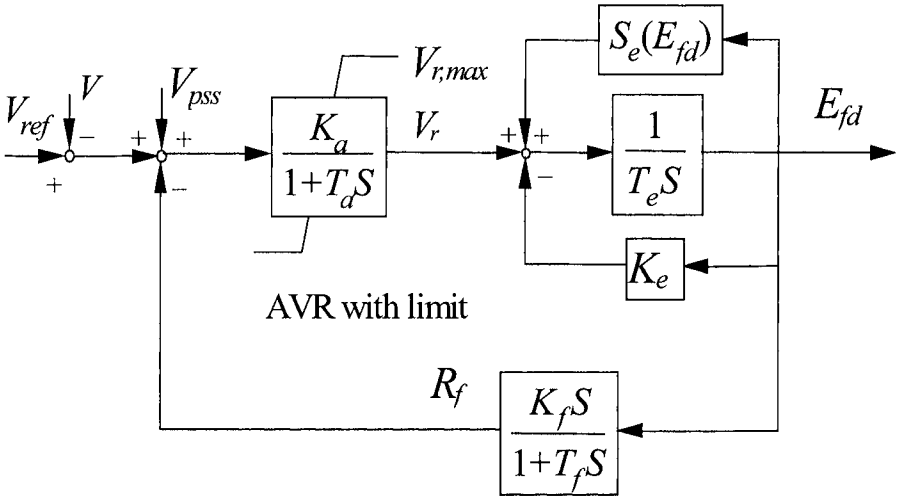

Fig. 3.22 The IEEE DC-1 model

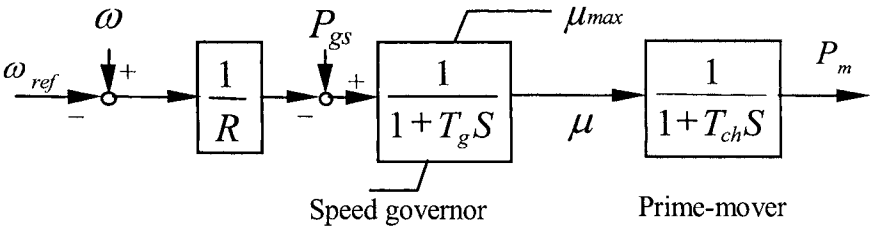

Fig. 3.23 The simplified speed governor and prime mover

3.8.1.4 Nonlinear load model

The voltage and frequency dependent load can be modeled as follows:

$$\begin{cases} P_{li} = P_{li0}(V_i / V_{i0})^{\alpha_i}[1 + K_{lpfi}(\omega_m - \omega_r)] \\ Q_{li} = Q_{li0}(V_i / V_{i0})^{\beta_i}[1 + K_{lqfi}(\omega_m - \omega_r)] \end{cases} \quad i = 1, \cdots, m \tag{3.36}$$

where P_{li0} and Q_{li0} are the active and reactive powers absorbed by the load at the nominal voltage V_i and frequency ω_r (=1.0). The frequency dependent term is included to prevent the equilibrium computation from divergence in case all the generators reach their maximum real power lim-

its due to load increase or generator outages. Here K_{lpf} and K_{lqf} are the load changing factors with respect to system frequency.

3.8.1.5 LTC model

Eqs.3.37 and 3.38 show the response of Load Tap Changer modeled as continuous. Assume the transformer is between bus i and bus j, then

$$V_j = rV_i \tag{3.37}$$

$$T_t \dot{r} = V_j^{ref} - V_j \tag{3.38}$$

where r is the tap ratio of an LTC; V_j^{ref} is the reference voltage at the LTC regulated bus j; T_t is the time constant.

3.8.1.6 Other Models

Generic Dynamic Load Model: Ref [20] proposed a generic load model to capture nonlinear characteristics as well load recovery. This model includes both steady state and transient load characteristics. Ref [21] further classifies this model in term of multiplicative generic model and additive generic model based on how load state variables affect the transient load characteristic. For additive generic model the corresponding equations that represent relevant responses are [21]:

Transient load response at particular bus i:

$$P_{liT} = P_{li0}[z_{Pi} + (\frac{Vi}{V_{i0}})^{\alpha_T}] \tag{3.39}$$

$$Q_{liT} = Q_{li0}[z_{Qi} + (\frac{Vi}{V_{i0}})^{\beta_T}] \tag{3.40}$$

Where the dyanmic state variables Z_{Pi} and Z_{Qi} represented by the following equations:

$$T_{Pi}\frac{d}{dt}z_{Pi} = -z_{Pi} + (\frac{Vi}{V_{i0}})^{\alpha_S} - (\frac{Vi}{V_{i0}})^{\alpha_T} \tag{3.41}$$

$$T_{Qi}\frac{d}{dt}z_{Qi} = -z_{Qi} + (\frac{Vi}{V_{i0}})^{\beta_S} - (\frac{Vi}{V_{i0}})^{\beta_T} \tag{3.42}$$

At steady state

$$P_{liS} = P_{li0}(\frac{Vi}{V_{i0}})^{\alpha_S} \tag{3.43}$$

$$Q_{liS} = Q_{li0}(\frac{Vi}{V_{i0}})^{\beta_S} \tag{3.44}$$

These models can be easily incorporated in general DAE formulation for equilibrium tracing or for time domain simulation. Time domain simulations for short term and for long term are discussed in chapter 6. Ref [21] also includes one chapter that provides wide coverage of various load aspects including the induction motor for voltage stability studies.

HVDC Models:

HVDC can also be easily incorporated into power flow. References [5, 7] provide a systematic presentation for power flow formulation for AC-DC power systems. These references cover AC –DC power flow solution both for single converter and multiterminal DC systems. Basically, there are real and reactive power mismatches at the converter terminal bus bars similar to AC power mismatches at particular AC bus. At converter terminal bus bar there are additional real and reactive power injections which are function of DC system variables and the converter AC terminal bus bar voltage. The variable corresponds to DC include: average DC voltage, converter DC current, firing angle of the converter, the converter transformer off- nominal tap ratio [7].

Ref [23] specifically discusses the comparison between point of collapse methods and continuation methods for large scale AC/DC systems. The detailed modeling related to AC-DC dynamic systems for point of collapse methods is discussed in ref [24]. This reference included inverter and converter control functions and showed voltage dependent current order limits affect the voltage stability margin of the system. This reference also observed Hopf bifurcation. For Hopf bifurcation, voltage dependent current order limit also played an important role.

In a recent paper [27] a single-infeed HVDC model is incorporated in combination with detailed synchronous machine modeling and excitation voltage control. The authors derived analytical expressions for power/voltage stability indices.

FACTS Device Models:

Reactive power plays an important role in voltage stability studies. Flexible AC Transmission Systems (FACTS), such as Static Var Compensator (SVC), Thyristor Controlled Series Capacitor (TCSC), Static Synchronous Compensator (STATCOM), and Unified Power Flow Controller (UPFC) can provide required fast control to improve voltage stability.

Reference [8] came with a general FACTS device model that is flexible enough to represent any FACTS device including the ones mentioned above. Functional characteristics of various FACTS devices are derived from Voltage Source Converter (VSC) model. This model can be used both for power flow as well stability studies. Ref [28] provided steady state models for SVC and TCSC with controls for voltage stability analysis.

3.8.1.7 Network power equations

Corresponding to the above models, the network equations can be written as:

$$\begin{cases} 0 = P_{gi} - (1 + K_{Li}\lambda)P_{li} - P_{ti} \\ 0 = Q_{gi} - (1 + K_{Li}\lambda)Q_{li} - Q_{ti} \end{cases} \quad i = 1, \cdots, n \tag{3.45}$$

Where

$$\begin{cases} P_{ti} = \sum_{k=1}^{n} V_i V_k Y_{ik} \cos(\theta_i - \theta_k - \varphi_{ik}) \\ Q_{ti} = \sum_{k=1}^{n} V_i V_k Y_{ik} \sin(\theta_i - \theta_k - \varphi_{ik}) \end{cases} \quad i = 1, \cdots, n \tag{3.46}$$

And

$$\begin{cases} P_{gi} = I_{di} V_i \sin(\delta_i - \theta_i) + I_{qi} V_i \cos(\delta_i - \theta_i) \\ Q_{gi} = I_{di} V_i \cos(\delta_i - \theta_i) - I_{qi} V_i \sin(\delta_i - \theta_i) \end{cases} \quad i = 1, \cdots, m \tag{3.47}$$

P_{gi} and Q_{gi} are the generator output powers, which are primarily determined by the inherent characteristics of the speed governor and the AVR regulations. They will change if real power generation rescheduling and secondary voltage control is applied. P_{ti} and Q_{ti} are the powers injected into the network at bus i. K_{Li} is load changing factor specified for bus i as mentioned in Section 3.8.3.

3.8.1.8 Power system DAE model

The above differential and algebraic equations are commonly known as a DAE representation of the power system. In a compact form, they can be simply represented by Eqs.3.13 and 3.14 as described in Section 3.6.

The state vector X and algebraic vector Y contain the following variables:

$$\begin{aligned} X &= (\delta, \omega, E_q^{'}, E_d^{'}, P_m, \mu, E_{fd}, V_r, R_f) \\ Y &= (V, \theta) \end{aligned} \tag{3.48}$$

The P in Eqs.3.13 and 3.14 can be further divided into control vector U and parameter vector Z

$$U = (V_{ref}, P_{gs}, \cdots), \quad Z = (P_l, Q_l) \tag{3.49}$$

In short, X contains all the system state variables; Y includes the algebraic variables; U is the control vector, whereas Z characterizes system loading condition.

3.8.2 Bifurcation modeling of power system dynamics

As discussed in Chapter 3, for a dynamic system parameterized by a single or a set of static parameters, bifurcations occur when the character of equilibrium changes within an arbitrary small local neighborhood of a critical parameter set. Those static parameters are defined as bifurcation parameters. Note that the prerequisite condition of bifurcation parameters is that their derivatives always equal zero. That is, they are out of dynamic variable set that characterize system state.

An extensive power system literature is available for the application of bifurcation related approach to voltage stability [9].

In power system DAE model, the change of equilibrium character with respect to bifurcation parameter is often effectively studied by analyzing changes of the eigenvalues of $A_{sys}(\lambda) = F_X - F_Y (G_Y)^{-1} G_X$ in response to parameter variations.

The various types of bifurcation points generally will form surfaces or manifold in the multidimensional parameter space. These surfaces serve in

the parameter space as boundaries separating regions where a certain type of system operation (as characterized by equilibria and trajectories) persists. A point on such a surface can be identified by a single bifurcation parameter $\lambda = \lambda_0$. These bifurcations are classified as codimension one. Only local codimension one bifurcations are discussed here.

3.8.2.1 Saddle-node bifurcation

Saddle-node bifurcation occurs when the Jacobian of the system $A_{sys}(\lambda_0)$ has a simple eigenvalue and there is no other eigenvalue on the imaginary axis. The equilibrium cease to exist when λ moves beyond λ_0. Correspondingly in the state space x, two equilibriums approach each other as λ approaches λ_0; then at λ_0 they fuse in a nonhyperbolic equilibrium (with a zero eigenvalue).

Under certain additional transversality (non-degenerate) conditions, the presence of the simple zero eigenvalue of the Jacobian essentially characterizes this bifurcation. In second-order systems, this bifurcation corresponds to the annihilation of a saddle point and a node, hence the name saddle-node bifurcation [10].

3.8.2.2 Hopf bifurcation

When Hopf bifurcation occurs, the Jacobian A_{sys} of the system has a simple pair of purely imaginary eigenvalues and there are no other eigenvalues on the imaginary axis. As the parameter changes, certain inequality conditions need to hold that ensure that this pair of critical eigenvalues crosses the imaginary axis. They can be formulated as

$$\frac{\partial}{\partial \lambda} \mathrm{Re}[\mu(\lambda)] \neq 0$$

when $\mathrm{Re}(\mu)$ denotes the real part of the eigenvalue μ, which moves across the imaginary axis, and $\partial/\partial\lambda$ denotes the derivative with respect to the bifurcation parameter λ.

Typically, this means that for $\lambda \neq \lambda_0$ the system has an equilibrium and a closed trajectory; a limit cycle exists near this equilibrium for one side of the parameters. This limit cycle can be unstable (or stable), that is, trajectories diverge (converge) from (to) it from both the inside and the outside.

The stable limit cycle corresponds to super critical Hopf bifurcation. The unstable limit cycle corresponds to sub critical Hopf bifurcation. The supercritical Hopf bifurcation corresponds to a transition in the system operating condition from a small-signal stable equilibrium point for $\lambda < \lambda_c$, and a small-signal stable limit cycle for $\lambda > \lambda c$. That is, when the system undergoes a supercritical Hopf bifurcation at $\lambda = \lambda c$, the system operating condition changes to sustained oscillation for $\lambda > \lambda c$. This type of supercritical Hopf bifurcation appears and played a fundamental role in the oscillating event experienced by Union Electric in 1992 [11, 12]. Ref [12] applied Hopf bifurcation analysis to large scale power system. The authors in this reference studied power system model in DAE form. Hopf related segments are traced by continuation based approaches. The critical eigenvalue is estimated either by power method or modified Arnoldi method.

3.8.3 Manifold models in power systems

Mathematical models of many, practically important scientific and technical problems involve differentiable manifolds. Differentiable manifolds are implicitly defined as the solution sets of systems of nonlinear equations. The mathematical basis for manifold and its numerical treatment are well established in the mathematical literature [3,13,15]. Following sections provide brief summary based on these references.

3.8.3.1 Manifold

Assume a dynamic system is represented by:

$$\dot{x} = F(x, \lambda) \qquad F : R^n \times R^d \rightarrow R^n \tag{3.50}$$

where F is a sufficiently smooth mapping, $x \in R^n$ is a state variable vector, $\lambda \in R^d$ is a parameter vector. The computational study of equilibria leads to nonlinear equations of 3.51.

$$F(x, \lambda) = 0 \tag{3.51}$$

As we see in the previous sections, it is of interest to determine the behavior of the solution under variation of λ. Here λ is a vector of parameters. The zero set $M = \{(x,\lambda) \in R^n \times R^d : F(x,\lambda) = 0\}$ has the structure of a submanifold of dimension d of the product $R^n \times R^d$ of state and parameter space. Computational techniques are well developed to find the critical point of interest on the manifold or any other dynamic behavior of interest. This approach can also be used in connection with equality constrained dynamical systems that are modeled by differential-algebraic equations (DAE) which are of interest to power system security analysis. Such DAE is known to be closely related to ordinary differential equations (ODE) on implicitly defined differentiable manifolds [13].

The basic computational problems arising in connection with any implicitly defined manifold is to come up with certain parameterizations. Finally it leads to solving certain set of nonlinear equations.

3.8.3.2 Natural parameterization

In many applications one can identify certain quantities that can be independently changed (for example constant load power change in power systems). This can be identified as parameter. This means that we have an intrinsic splitting, which includes a d-dimensional parameter space Λ and a state space X of dimension n.

$$X \oplus \Lambda \quad \text{and} \quad \dim(\Lambda) = d$$

This is a natural parameter splitting of original variable space. One can use the parameter space Λ as the coordinate space of a local coordinate system.

For example for power system we can identified parameters involved in power flow type formulation as well DAE type formulation. For some cases, the natural parameterization may be not suitable to be a local parameterization, in which cases singularity is always encountered while solving for the solution of nonlinear equation system.

3.8.3.3 Local parameterization

Rheinboldt [13] described mathematics behind the local parameterization to trace the equilibrium curve. The local parameterization could avoid the singularity encountered by the natural parameterization. The procedure for one parameter problem is described here. Continuation methods produce a sequence of solutions for changing parameter. Local parameterization pro-

vides a way to trace this path successfully. Local parameterization at a given step requires a nonzero vector $e \in R^n$ such that

$$e \notin rangeDF\ (x)^T \tag{3.52}$$

Basically (3.52) implies e should not be normal vector of M at x.

Then the local parameterization involves solving the following augmented system of equations for a given value of η which is a scalar.

$$H(x) \equiv \begin{pmatrix} F(x) \\ e^T (x - x_c) \end{pmatrix} = \begin{pmatrix} 0 \\ \eta \end{pmatrix} \tag{3.53}$$

The Jacobian

$$DH(x) = \begin{pmatrix} DF(x) \\ e^T \end{pmatrix}$$

is nonsingular in an open neighborhood of $x = x_c$ [13].

This general setting becomes background material for the continuation power flow discussed in section 3.4. Basically DH(x) can be related to the augmented jacobian J_{aug}. How to choose vector e and the scalar parameter η are discussed in the predictor and corrector tracing process in the same section.

This basic manifold approach can be exploited to identify and trace voltage stability boundaries

Power system equilibrium manifold is defined in this chapter for power system equilibrium tracing.

Saddle node bifurcation related voltage stability margin boundary manifold is defined in Chapter 5 for voltage stability margin boundary tracing.

3.8.4 Equilibrium manifold Tracing of power systems

Simultaneously solving for X and Y will enable us to avoid the assumptions used in power flow. This leads us to the question whether it is possible to solve for X and Y directly and simultaneously from Eqs.3.13 and 3.14 at equilibrium, i.e.,

$$0 = F(X,Y,U,Z) \tag{3.54}$$

$$0 = G(X,Y,U,Z) \tag{3.55}$$

The immediate concern is whether the Newton's method would work with as good convergence as that in the power flow.

As mentioned earlier, the release of slack bus generation is used in power flow so that network losses corresponding to a set of system voltages are not causing convergence trouble during iterations. In the complete description of the system at equilibrium state, this compensation becomes possible without the necessity of removing the slack bus power balance equations. With the description of the system at steady state by 3.54 and 3.55, generation at terminal interface to the network is now a function of system states (see Eqs.3.47). The governor frequency regulation together with the boiler valve control, as described by Eqs.3.35 and 3.34, interacts with the network real power balance constraints, through mechanical power P_{Mi} (Eqs.3.23 and 3.34), to adjust the interface generation P_{gi} so that real power losses are automatically compensated by regulating the system frequency. Similarly, the automatic voltage regulator (described by Eqs.3.14 and 3.16) interacts with the network reactive power balance constraints, through E_{fdi} to adjust Q_{gi} so that reactive power losses are compensated by regulating terminal bus voltage V_i. In regard to PV bus assumption, it is not needed any more since AVR is actually represented.

Based on the above analysis, it is possible to solver for X and Y simultaneously by directly applying Newton's method to Eqs.3.54 and 3.55. Further, in the following section, we will show how we can incorporate

this into continuation and apply the resultant simultaneous equilibria tracing technique to voltage collapse identification. Overall solution methodology is given in the sequel.

Eqs.3.54 and 3.55 define the equilibrium manifold of power system. The conventional power flow solution is simply a point on this manifold corresponding to certain condition. It could be thought of as an intersection point of the equilibrium manifold and a cut line (or hyper-plane) defined by system condition. Naturally power system condition is parameterized by control variables U and loading condition Z that present in the power system DAE model.

The equilibrium is the solution of a set of nonlinear equations which are introduced in the previous sections. It could be calculated by Gauss-Sedel method or Newton-Raphson method (or their derivatives). Newton-Raphson type of method is widely used due to its super linear convergence rate. But when load stress on power system is increased, both methods can diverge however close the initial guess is. This is caused by singularity of the total system Jacobian of (Eqs.3.54 and 3.55).

Similar approach to the continuation power flow presented in Section 3.4 can be also applied to trace the total equilibrium as defined by (Eqs. 3.54 and 3.55).

To trace this equilibrium, first we need an initial starting point. Next section provides details related to this initial condition.

3.8.5 Initialization for power system equilibrium tracing

To start power system equilibrium tracing, we need initial conditions that are defined by following variables at all buses $\delta, \omega, E_q^{'}$, $E_d^{'}, E_{fd}, V_r, R_f$, I_d, I_q, V, θ. Solution from power flow provides V, θ at all buses. The remaining values are obtained as shown as follows [6].

The first step in computing the initial conditions is to obtain the generator currents from Eq.3.55:

$$I_{G_i} e^{j\gamma_i} = \frac{P_{G_i} - Q_{G_i}}{V_i e^{-j\theta_i}} \tag{3.56}$$

and the relative machine rotor angels from manipulation of the stator and flux equations

$$\delta_i = \text{angle of } (V_i e^{j\theta_i} + (R_{s_i} + jX_{q_i})I_{G_i} e^{j\gamma_i}) \tag{3.57}$$

With these quantities, the remaining dynamic and algebraic states can be obtained by

$$I_{d_i} + jI_{q_i} = I_{G_i} e^{j(\gamma_i - \delta_i + 90^\circ)} \tag{3.58}$$

$$V_{d_i} + jV_{q_i} = V_i e^{j(\theta_i - \delta_i + 90^\circ)} \tag{3.59}$$

followed by E_{fd} from the stator and flux equation

$$E_{fd_i} = X_{d_i} I_{d_i} + V_{q_i} + R_{s_i} I_{q_i} \tag{3.60}$$

With this field voltage, R_{f_i}, V_{R_i} and V_{ref_i} can be found from the exciter equations as

$$R_{f_i} = \frac{K_{f_i}}{T_{f_i}} E_{fd_i} \tag{3.61}$$

$$V_{r_i} = (K_{e_i} + S_{e_i}(E_{fd_i}))E_{fd_i} \tag{3.62}$$

$$V_{ref_i} = V_i + \frac{V_{r_i}}{K_{a_i}} \tag{3.63}$$

This initial value of E'_{qi} and E'_{di} are then found from the flux equations:

$$E'_{qi} = -(X_{d_i} - X'_{d_i})I_{d_i} + E_{fd_i} \tag{3.64}$$

$$E'_{di} = -(X_{q_i} - X'_{q_i})I_{q_i} \tag{3.65}$$

This completes the computation of all dynamic state initial conditions.

3.8.6 Continuation method with local parametrization

This section extends the application of the continuation method described in Section 3.4 to the power system DAE formulation. The system equilibrium manifold defined by Eqs.3.54 and 3.55 could be traced, according to a scheduled scenario parameterized by λ, from base case up to the point where voltage collapse associated with the saddle node bifurcation occurs.

The same predictor and corrector process described in Section 3.4 can be applied here. Then the tangent vector is solved from

$$\begin{bmatrix} F_X & F_Y & F_\lambda \\ G_X & G_Y & G_\lambda \\ & e_k^T & \end{bmatrix} \begin{bmatrix} dX \\ dY \\ d\lambda \end{bmatrix} = \begin{bmatrix} 0 \\ 0 \\ \pm 1 \end{bmatrix} \tag{3.66}$$

Once the prediction is made with the tangent vector, the following correction is performed to find the equilibrium point.

$$\begin{bmatrix} F_X & F_Y & F_\lambda \\ G_X & G_Y & G_\lambda \\ & e_k^T & \end{bmatrix} \begin{bmatrix} \Delta X \\ \Delta Y \\ \Delta\lambda \end{bmatrix} = -\begin{bmatrix} F \\ G \\ 0 \end{bmatrix} \tag{3.67}$$

where $[dX^T, dY^T, d\lambda]^T$ is the tangent vector. e_k is a column unit vector with all the elements equal to zero except for the k^{th} one, which corresponds to the current continuation parameter. Since F_λ and G_λ can not be null vectors at the same time even at the base case (λ =0), the singularity of the augmented Jacobian matrix can be easily avoided by appropriately selection of the continuation parameter. To speed up the computation, the same Jacobian can be used in Eqs.3.66 and 3.67.

Since λ is introduced to parameterize the system generation and load level, it increases monotonically to the maximum value. Hence $d\lambda$ is positive before λ reaches its maximum, and negative afterwards. Null $d\lambda$ indicates that the system total Jacobian matrix is singular. This can be clearly seen as follows.

3.8.7 Linerization of power system DAE

When the parameter in Eqs.3.13 and 3.14 is varied, the corresponding state vector X and the eigenvalues of the system matrix evaluated on this path change accordingly.

Linearization of Eqs.3.13 and 3.14 at the equilibrium point with specified U and Z is presented as follows:

$$\begin{bmatrix} \Delta \dot{X} \\ 0 \end{bmatrix} = \begin{bmatrix} F_X & F_Y \\ G_X & G_Y \end{bmatrix} \begin{bmatrix} \Delta X \\ \Delta Y \end{bmatrix} = J_{total} \begin{bmatrix} \Delta X \\ \Delta Y \end{bmatrix} \tag{3.68}$$

Matrices F_X, F_Y, G_X, and G_Y contain first derivatives of F and G with respect to X and Y, evaluated at the equilibrium point.

Note that matrix G_Y is an algebraic Jacobia matrix that contains the power flow Jacobian matrix. In the above equation, if det(G_Y) does not equal zero

$$\Delta Y = -G_Y^{-1} G_X \Delta X \tag{3.69}$$

Substituing in (3.68) results in

$$\Delta \dot{X} = A_{sys} \Delta X \tag{3.70}$$

$$A_{sys} = F_X - F_Y G_Y^{-1} G_X \tag{3.71}$$

The essential small-disturbance dynamic characteristics of a structure-preserving model are expressed in terms of eigen-properties of the reduced system matrix A_{sys}. This matrix is called dynamic system state matrix.

Eigenvalue analysis of A_{sys},will give small signal stability information of the current equilibrium point under small disturbances. At voltage collapse, the system loses the ability to supply enough power to a heavily loaded network. At that point, the so-called saddle node bifurcation occurs which is described by the movement of one eigenvalue of A_{sys} on the real axis crossing the origin from the left half complex plane. Eigenvalue computation will help detect this movement, participation factor studies will show how bus voltages participate in this collapse mode, and sensitivity analysis will show the parameter influence on this critical situation [5].

At saddle node bifurcation which leads to voltage collapse, one of the eigenvalue of A_{sys} becomes zero. Equivalently, the determinant of A_{sys} equal zero. From matrix theory, we know that,

$$\begin{aligned}\det(J_{total}) &= \det\begin{bmatrix} F_X & F_Y \\ G_X & G_Y \end{bmatrix} = \det(F_X - F_Y G_Y^{-1} G_X)\det(G_Y) \\ &= \det(A_{sys})\det(G_Y)\end{aligned} \tag{3.72}$$

So if G_Y is nonsingular, the determinant of A_{sys} becomes zero if and only if the determinant of J_{total} is zero. This is the Schur formula. J_{total} is very sparse and thus allow efficient handling using sparse techniques. Therefor detection of the singularity of A_{sys} is equivalent to the detection of the singularity of J_{total}.

3.8.8 Detection of Saddle Node Bifurcation with System Total Jacobian

Proposition 1: When G_Y^{-1} exists and $u_X \neq 0$, then the following equivalent condition is valid

$$A_{sys} u_X = \lambda u_X \tag{3.73}$$

if and only if

$$\begin{bmatrix} F_X - \lambda I & F_Y \\ G_X & G_Y \end{bmatrix}\begin{bmatrix} u_X \\ u_Y \end{bmatrix} = 0 \tag{3.74}$$

where

$$u_Y = -G_Y^{-1} G_X u_X \tag{3.75}$$

We *define the extended eigenvector* $u = \begin{bmatrix} u_X^T & u_Y^T \end{bmatrix}^T$.

Proof:

1. Assume $A_{sys} u_X = \lambda u_X$, i.e.,

$$(F_X - F_Y G_Y^{-1} G_X) u_X = \lambda u_X \tag{3.76}$$

From L.H.S of Eq.3.74

$$\begin{bmatrix} F_X - \lambda I & F_Y \\ G_X & G_Y \end{bmatrix}\begin{bmatrix} u_X \\ u_Y \end{bmatrix} = \begin{bmatrix} (F_X - \lambda I)u_X + F_X u_Y \\ G_X u_X + G_Y u_Y \end{bmatrix} \tag{3.77}$$
$$= \begin{bmatrix} (F_X - \lambda I)u_X - F_X G_Y^{-1} G_X u_X \\ G_X u_X - G_Y G_Y^{-1} G_X u_X \end{bmatrix} = \begin{bmatrix} (F_X - F_X G_Y^{-1} G_X)u_X - \lambda u_X \\ 0 \end{bmatrix} = 0$$

Substitution of $u_Y = -G_Y^{-1} G_X u_X$ in the above equation verifies Eq.3.74.
Or

2. Assume

$$\begin{bmatrix} F_X - \lambda I & F_Y \\ G_X & G_Y \end{bmatrix}\begin{bmatrix} u_X \\ u_Y \end{bmatrix} = 0 \tag{3.78}$$

$$\begin{bmatrix} (F_X - \lambda I)u_X + F_X u_Y \\ G_X u_X + G_Y u_Y \end{bmatrix} = 0 \tag{3.79}$$

From the second item in Eq.3.79, $u_Y = -G_Y^{-1} G_X u_X$. Substitute this into the first item

$$(F_X - \lambda I)u_X - F_X G_Y^{-1} G_X u_X = 0 \tag{3.80}$$

After rearrangement, based on the definition of A_{sys}

$$A_{sys} u_X = \lambda u_X \tag{3.81}$$

is obtained. This concludes the proof for proposition 1.

□

From Eq.3.74, the total Jacobian matrix

$$A_{total} = \begin{bmatrix} F_X & F_Y \\ G_X & G_Y \end{bmatrix}$$

can be used to detect either Saddle node or Hopf bifurcation.

3.8.8.1 Detection of saddle-node bifurcation

From proposition 1, the condition

$$\begin{bmatrix} F_X & F_Y \\ G_X & G_Y \end{bmatrix}\begin{bmatrix} u_X \\ u_Y \end{bmatrix} = 0 \tag{3.82}$$

can be utilized to detect Saddle node bifurcation, that is, to detect the singularity of the total Jacobian matrix.

During the direct equilibrium tracing, the saddle node bifurcation point can be readily identified by utilizing a cut function, without computing eigenvalues [13,15].

A cut function for Saddle node related fold bifurcation can be implicitly defined as $\gamma_{SNB}(x)$ in the following equation:

$$\begin{bmatrix} F_X & F_Y & e_k \\ G_X & G_Y & \\ e_j^T & & 0 \end{bmatrix} \begin{bmatrix} u_X^0 \\ u_Y^0 \\ \gamma_{SNB} \end{bmatrix} + \begin{bmatrix} 0 \\ 0 \\ 1 \end{bmatrix} = 0 \tag{3.83}$$

where we denote $u^0 = [u_X^0 \quad u_Y^0]^T$. Or equivalently,

$$\begin{bmatrix} F_X & F_Y & e_k \\ G_X & G_Y & \\ e_j^T & & 0 \end{bmatrix}^T \begin{bmatrix} v_X^0 \\ v_Y^0 \\ \gamma_{SNB} \end{bmatrix} + \begin{bmatrix} 0 \\ 0 \\ 1 \end{bmatrix} = 0 \tag{3.84}$$

where we denote $v^0 = [v_X^0 \quad v_Y^0]^T$.

At the fold point, the cut set condition is satisfied, that is $\gamma_{SNB}(X, Y, \alpha, \beta) = 0$.

At each continuation step, γ_{SNB} is checked. If γ_{SNB} changes sign, Saddle node bifurcation has just been passed. This γ_{SNB} is nothing but $d\lambda$ [16].

If null $d\lambda$ is detected at some step, then Eq.3.36 reduces to

$$\begin{bmatrix} F_X & F_Y \\ G_X & G_Y \end{bmatrix} \begin{bmatrix} dX \\ dY \end{bmatrix} \approx \begin{bmatrix} J_{total} \end{bmatrix} \begin{bmatrix} dX \\ dY \end{bmatrix} = \begin{bmatrix} 0 \\ 0 \end{bmatrix} \tag{3.85}$$

Since

$$\begin{bmatrix} e_k^T \end{bmatrix} \begin{bmatrix} dX \\ dY \\ 0 \end{bmatrix} = \begin{bmatrix} 0 \\ 0 \\ \pm 1 \end{bmatrix} \tag{3.86}$$

So one of the components of dX or dY is ± 1, not a null vector, Eq.3.85 hence implies the total system Jacobian J_{total} singular. As mentioned before, from Eq.3.72, the singularity of J_{total} coincides with the singularity of A_{sys} if G_Y is nonsingular.

The singularity of A_{sys} implies it has a null eigenvalue at the current step. Therefore null $d\lambda$ exactly signifies a saddle node bifurcation. Thus it can readily identify the saddle node bifurcation point by equivalently detecting null $d\lambda$ during the direct equilibrium tracing, without formation of A_{sys} and computing its eigenvalues.

However, when system limits are considered, sometimes we could not capture the null $d\lambda$ point even using a very small step length. It most probably means an immediate voltage collapse encountered due to some generators hitting their limits [17]. On the other hand, in order to investigate the voltage collapse mechanisms or to develop an effective control strategy against voltage collapse, the critical eigenvalue responsible for the voltage collapse may be needed.

In general, there is no simple way to capture the critical eigenvalue at an immediate voltage collapse point. However, this critical eigenvalue can readily be detected via simultaneous equilibrium tracing. That is, we can use the general tracing scheme illustrated in Fig.3.24 to locate the saddle node bifurcation point where the critical eigenvalue crosses the origin on the complex plane.

First, we use a relatively large step size to trace the system equilibrium diagram BC_{im} until the negative $d\lambda$ is detected at point C_{im}. Then we should change the tracing direction and continue the process with a smaller step size up to the saddle node bifurcation point C_{snb} where null $d\lambda$ could be easily detected. If the traced equilibrium diagram is the same as depicted in Fig.3.24, we can conclude that the point C_{im} is the system immediate voltage collapse point. Otherwise, in case null $d\lambda$ is detected but the saddle node bifurcation point C_{snb} is sitting on the BC_{im} diagram, it means that the voltage collapse results from the saddle node bifurcation rather than the system limits. Note that the tracing process always stops at the saddle node bifurcation point. The solid curve with arrows indicates the tracing path and direction.

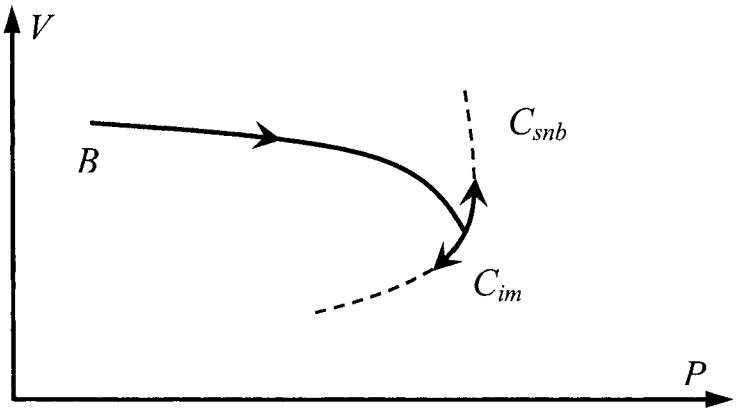

Fig. 3.24 Illustration of direct equilibrium tracing process

3.8.9 Limits implementation

It is very important to reasonably represent the system limits when studying voltage stability. In fact, voltage collapse occurs more than often as a consequence of limited local reactive power supply. When the system loses the ability to further meet the load demand in a heavily stressed network, the cascaded hitting of limits usually leads to system collapse. There are basically two types of limits to be considered. One is the governor limit, and the other is the AVR output limit. For voltage stability, the latter usually plays a more important role.

3.8.9.1 Governor limits

The governor limits are implemented by regulating the real power generation/load settings. Those generators which hit $P_{gsi}^{\max}$ will then be forced to stay at maximum, and no longer allowed to further pick up the system load increase.

3.8.9.2 AVR limits

The automatic voltage regulator (AVR) controls the terminal voltage of the synchronous machine. It indirectly controls the reactive power output by regulating the AVR output voltage V_r. In the new formulation, we are able

to directly implement the limits which are usually given to restrict the output of the voltage regulator. Forcing the AVR output voltage at a particular value will directly control the rotor current to stay below limits and indirectly control the reactive generation. This can be shown as follows. At an equilibrium state, the AVR output voltage is related to the synchronous machine rotor current as

$$\begin{aligned} V_{ri} &= (K_{ei} + S_{ei})E_{fdi} \\ &= (K_{ei} + S_{ei})E_{qi} \\ &= (K_{ei} + S_{ei})X_{adi}I_{fdi} \end{aligned} \tag{3.87}$$

where E_{qi} is the generator's internal induced quadrature axis voltage [18]. So if we ignore the saturation effect, the rotor current is proportional tor V_{ri}, which verifies the first half of the above statement. A machine's reactive power output can be written as:

$$Q_{Gi} = \frac{V_i E_{qi}}{X_{di}} \cos(\delta_i - \theta_i) - V_i^2 \left(\frac{\cos^2(\delta_i - \theta_i)}{X_{di}} + \frac{\sin^2(\delta_i - \theta_i)}{X_{qi}}\right) \tag{3.88}$$

When V_{ri} is fixed at a certain value, the reactive power will then be limited indirectly, at lease not increase exponentially when approaching voltage collapse. This shows the second half of the previous statement.

Once the AVR of a generator hits the limit, it loses the ability to adjust V_{ri} and thus Q_{Gi} to meet the load increase. The AVR has to be set so that V_{ri} stays at the limiting value. Referring to Eq.3.32, the dynamic differential equation will be dropped and will not be included for stability analysis. This is obvious if one recalls the definition of stability from control theory. That is, the limited dynamic state will stay as a constant, and it no longer participates in the dynamic response of the system. If we solve the remaining equations which provide the DAE description of the system with the same control inputs, we may not be able to find a solution. This is because, when the system load further increases, in order to continuously keep V_{ri} at the limiting value, the corresponding excitation reference voltage V_{refi} may have to be reduced. The decrease of the exciter reference voltage reflects the inability of the generator to keep pace with the load increase. In the conventional two-step based equilibria tracing ap-

proach, this would require a new power flow solution with a different set of generation and/or voltage specifications for the PV buses. After this, the X variables are then calculated and the control inputs including the exciter reference voltage will then be updated to a new smaller value in this case. As mentioned in the first section of this chapter, this causes the problem of inconsistent description of the generators. In the new formulation, when some new limits are hit, this update of control settings can be done automatically during continuation. To do so, we include the following equation, which is nothing but the right hand side of Eq.3.32 with V_{ri} at its maximum.

$$0 = \frac{1}{T_{ai}}(-V_{ri}^{\max} + K_{ai}(V_{refi} - V_i - R_{fi})) \triangleq f_i^{AVR+} \tag{3.89}$$

If a new limit is found to be violated at the end of the current correction, the following Jacobian will then be used in the immediate correction to update the input exciter reference voltage.

$$-\begin{bmatrix} \overline{F}_{\overline{X}} & \overline{F}_Y & 0 & \overline{F}_\alpha \\ G_{\overline{X}_i} & G_Y & 0 & G_\alpha \\ f_{i\overline{X}}^{AVR+} & f_{iY}^{AVR+} & f_{iV_{ref}}^{AVR+} & 0 \\ & e_k^T & & \end{bmatrix} \begin{bmatrix} \Delta\overline{X} \\ \Delta Y \\ \Delta V_{refi} \\ \Delta\alpha \end{bmatrix} = \begin{bmatrix} \overline{F} \\ G \\ f_i^{AVR+} \\ 0 \end{bmatrix} \tag{3.90}$$

where $\overline{F} = \{F\} - \{f_i^{AVR}\}$ and $\overline{X} = \{X\} - \{V_{ri}\}$ and $f_{iV_{ref}}^{AVR+} \triangleq \partial f_i^{AVR+} / \partial V_{refi}$. After this, if no new limits are violated, the following equation will then be used for subsequent correctors:

$$-\begin{bmatrix} \overline{F}_{\overline{X}} & \overline{F}_Y & 0 & \overline{F}_\lambda \\ G_{\overline{X}} & G_Y & 0 & G_\lambda \\ f_{i\overline{X}}^{AVR+} & f_{iY}^{AVR+} & 10^{15} & 0 \\ & e_k^T & & \end{bmatrix} \begin{bmatrix} \Delta\overline{X} \\ \Delta Y \\ \Delta V_{ri} \\ \Delta\lambda \end{bmatrix} = \begin{bmatrix} \overline{F} \\ G \\ 0 \\ 0 \end{bmatrix} \tag{3.91}$$

Once the limit is hit, the predictor equation from then on is changed to

$$-\begin{bmatrix} \overline{F}_{\overline{X}} & \overline{F}_{Y} & 0 & \overline{F}_{\lambda} \\ G_{\overline{X}} & G_{Y} & 0 & G_{\lambda} \\ f_{i\overline{X}}^{AVR+} & f_{iY}^{AVR+} & 10^{15} & 0 \\ & e_k^T & & \end{bmatrix} \begin{bmatrix} d\overline{X} \\ dY \\ dV_{ri} \\ d\lambda \end{bmatrix} = \begin{bmatrix} 0 \\ 0 \\ 0 \\ \pm 1 \end{bmatrix} \tag{3.92}$$

The large number is used to keep the size of the matrix unchanged which provides programming ease. And by using this Jacobian, we observe that neither the AVR output voltage nor the input exciter reference voltage is updated during the prediction process. This makes sure that we get the tangent of the equilibrium curve corresponding to the current input settings while satisfying the limits already encountered. The above analysis is illustrated in Fig.3.25.

When $d\lambda$ is zero, from Eq.3.92:

$$det\begin{pmatrix} \overline{F}_{\overline{X}} & \overline{F}_{Y} & 0 \\ G_{\overline{X}} & G_{Y} & 0 \\ f_{\overline{X}}^{AVR+} & f_{Y}^{AVR+} & 10^{15} I \end{pmatrix} = 0 \tag{3.93}$$

And we have

$$\det\begin{pmatrix} \overline{F}_{\overline{X}} & \overline{F}_{Y} & 0 \\ G_{\overline{X}} & G_{Y} & 0 \\ f_{\overline{X}}^{AVR+} & f_{Y}^{AVR+} & 10^{15} I \end{pmatrix} = \det\begin{pmatrix} \overline{F}_{\overline{X}} & \overline{F}_{Y} \\ G_{\overline{X}} & G_{Y} \end{pmatrix} \det(10^{15} I) \tag{3.94}$$

Thus we observe that $d\lambda = 0$ again signifies saddle node bifurcation of the DAE model.

The above derivation [19] provides the validity of using the iterative continuation of Jacobian (Eq.3.92) in simultaneous equilibria tracing to identify voltage collapse, both before and after hitting AVR limits. In Chapter 4, we will see that the continuation Jacobian can also be used for studying the sensitivity of the saddle node bifurcation of the DAE model.

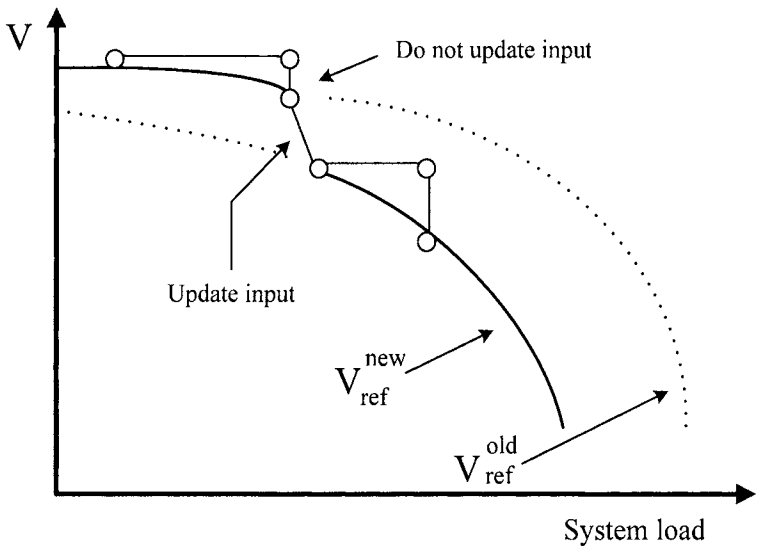

Fig. 3.25 Limits implementation during continuation

3.9 Numerical examples for EQTP

EQTP Scenario Description:

In the EQTP simulation, the scenario is similar to scenario 1 in CPF. Loads at the same 8 buses are increased, while the increased load is picked up by the same 9 generators. And both load and generator are increased proportionally by their initial load and generation levels.

For this scenario the variations of load bus voltages, generator real powers, and reactive powers for changing load are shown in Figs. 3.26, 3.27, and 3.28 respectively.

As explained in the previous sections, the automatic voltage regulator regulates the generator terminal voltage and its reactive power output of the network. The speed governor adjusts the real power generation and frequency to meet load increase. Because all these devices are modeled in detail, we are able to observe how the synchronous machines interact with the network, both before and after hitting the limits. The inability of indefinitely supplying power through the network to the load centers, as consequence of control system or machine capacity limitations and network loadability restrictions, will ultimately lead to system voltage collapse.

For all the generators which hit their AVR output voltage limits, the terminal voltage, AVR output voltage, reactive power generation, and exciter reference voltage have similar response profiles. Therefore we take the generator at bus 30 bus as the example for the explanation.

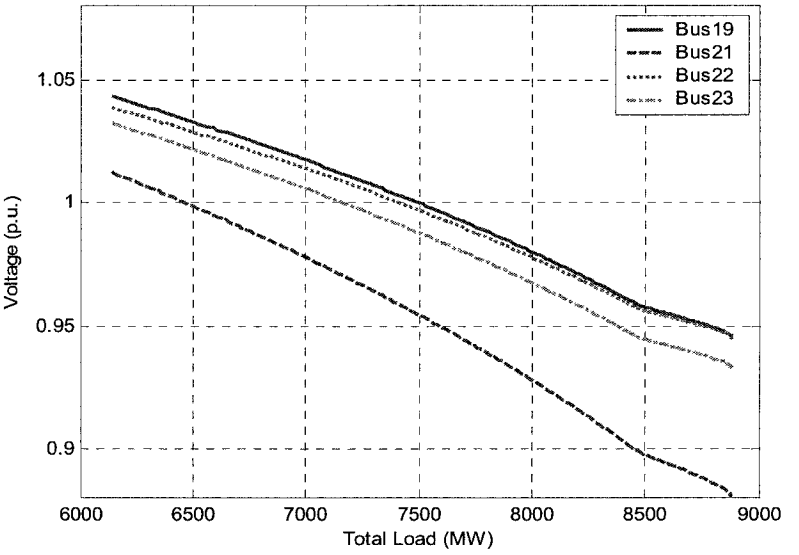

Fig. 3.26 V vs. P_{total}

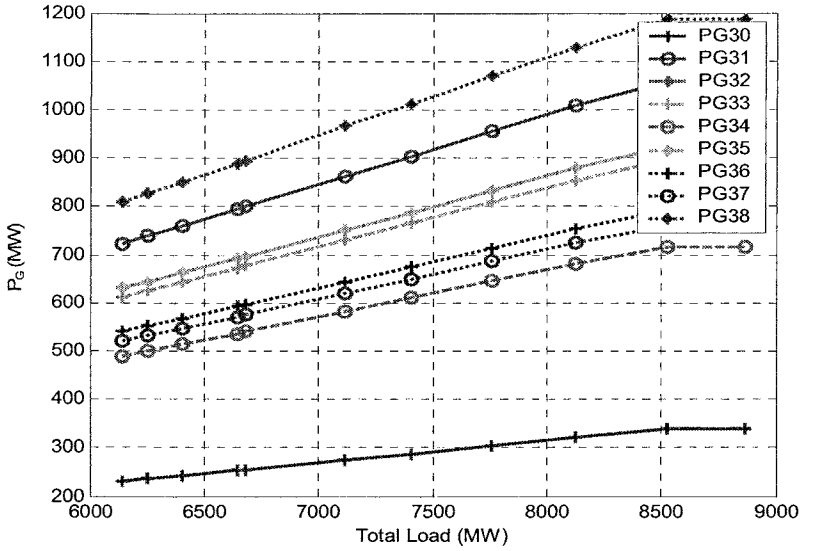

Fig. 3.27 P_G vs. P_{total}

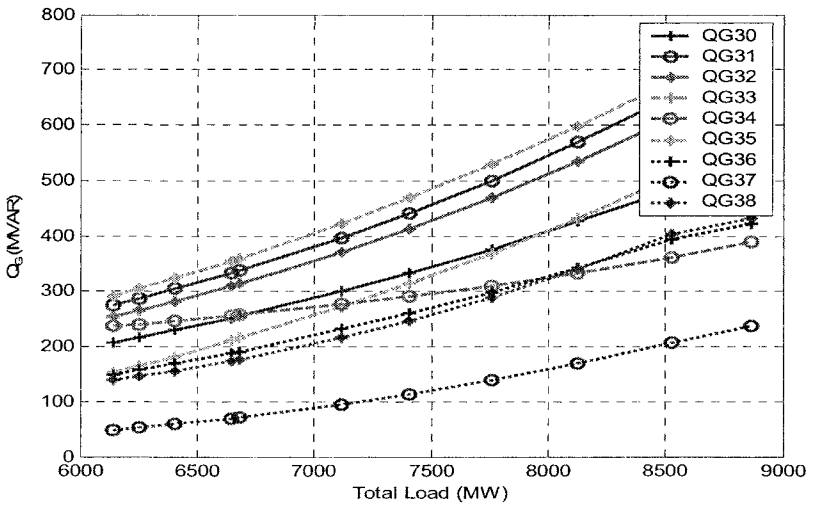

Fig. 3.28 Q_G vs. P_{total}

Fig 3.29 shows that, before hitting its AVR output limit, the voltage regulator can maintain a fairly high and steady terminal voltage. When the sys-

tem total load exceeds 8845MW, AVR output voltage as shown in Fig. 3.30 hits the maximum value and the terminal voltage experiences a noticeable drop.

Fig. 3.31 shows the profile of reactive power generation at bus 32. A sudden slowing down of the increase in the reactive power generation occurs when the AVR output limit is hit. From this point on, fixing the AVR output voltage makes the terminal reactive power generation to decrease slightly.

Figs. 3.30 and 3.32 are the AVR output and exciter reference voltages of the generator at bus 32.

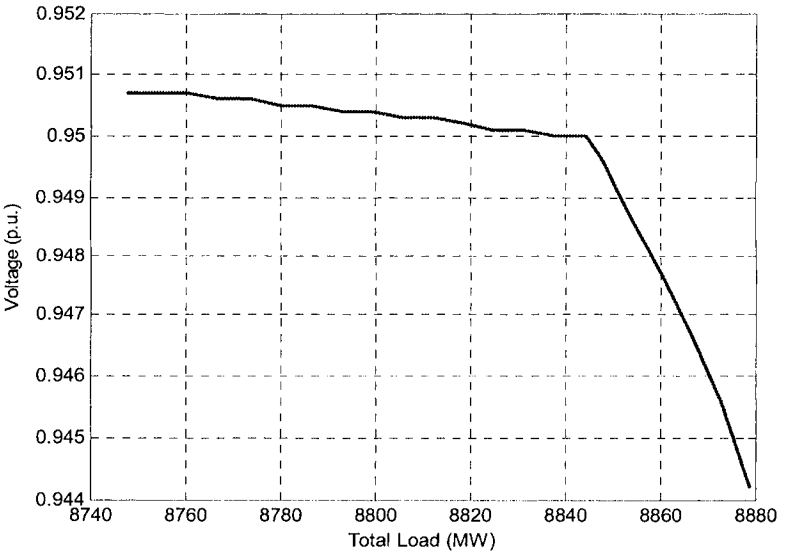

Fig. 3.29 Voltage at Generator Bus 32

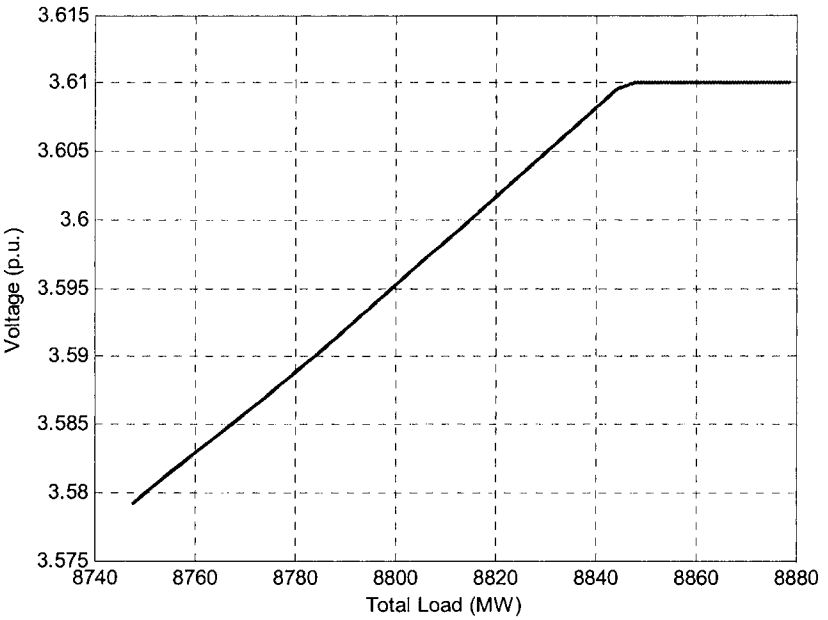

Fig. 3.30 AVR Output Voltage Vr at Bus 32

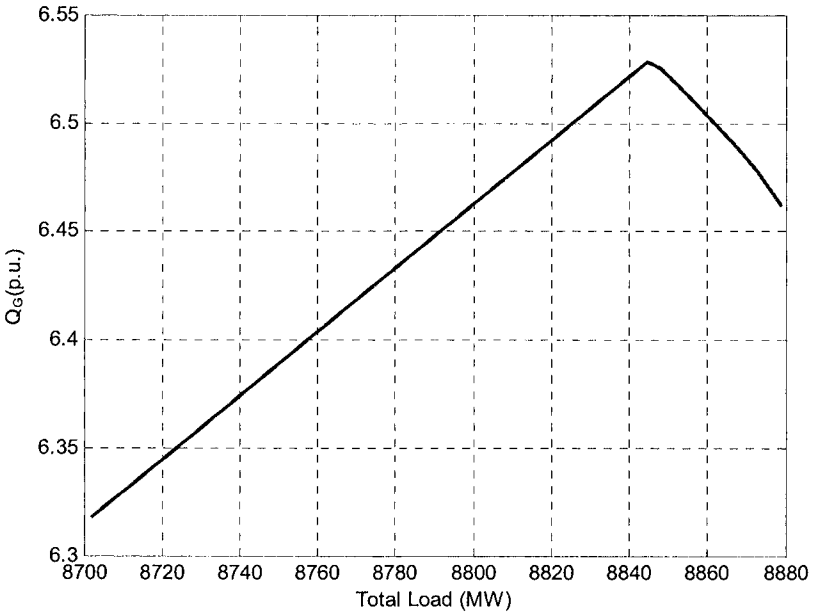

Fig. 3.31 Reactive power generation at bus 32

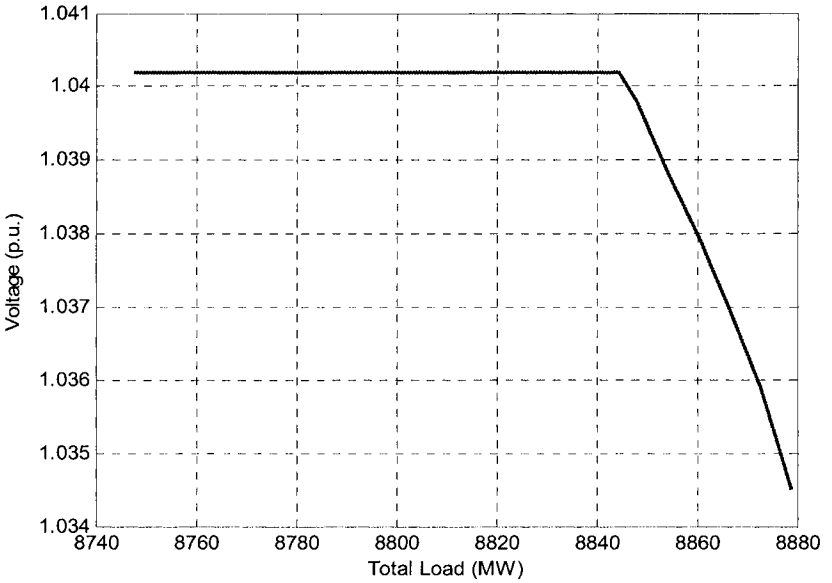

Fig. 3.32 Exciter reference voltage at bus 32

The governor associated with generator at bus 30 is the first to reach its limit when the system loading level is 8523 MW. Fig. 3.33 shows the governor setting value. At a system loading level of 8523 MW, when most of the governors hit their limits, the system frequency experiences sag as shown in Fig. 3.34.

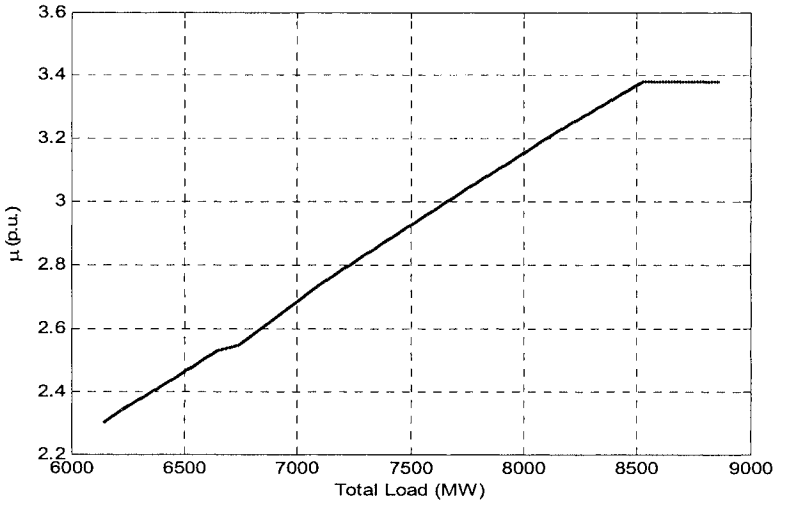

Fig. 3.33 Governor Response of Generator at Bus 30

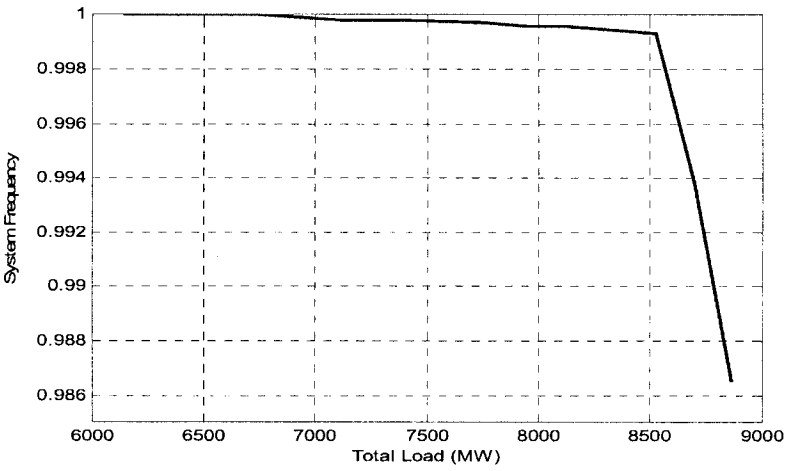

Fig. 3.34 System Frequency Response

As mentioned before various versions of continuation power flow methods are proposed in the literature [22-26]. These methods depend on the type of parameterization strategies. Continuation based approaches can also be used for critical eigenvalue tracing. References [12, 29, 30] discuss the application of continuation based approaches for eigenvalue tracing.

References

[1] Allgower, E. L. and Gearg, K., *Numerical Continuation Methods.* Springer-Verlag, 1990

[2] Seydel, R., *From equilibrium to chaos,* Elsevier Science, 1988

[3] Rheinboldt, W.C., "Solutions fields of nonlinear equations and continuation methods, " *SIAM J. Num. Anal.*, Vol. 17, 1980, pp. 221-237

[4a] Christy, C.D., *Analysis of steady state voltage stability in large scale power systems,* M.S. Thesis, Iowa State University, Ames, IA, 1990

[4b] Ajjarapu, V. and Christy, Colin, "The Continuation Power Flow: A Tool to Study Steady State Voltage Stability," *IEEE Transactions on Power Systems*, Vol. 7, No. 1, pp. 416-423, Feb. 1992

[5] Kundur, P., *Power system stability and control,* McGraw Hill, 1994

[6] Sauer, P. W., Pai, M. A., "Power system steady-state stability and the load flow jacobian, " *IEEE Trans. on power systems*, 1990, 1374-1383

[7] Arrillaga, J., Smith, B., *AC-DC power systems analysis,* The Institution of Electrical Engineers, London, UK, 1998

[8] Arabi, S. and Kundur, P.,"A versatile FACTS device model for power flow and stability simulations " IEEE Transactions on Power Systems , Volume 11, Issue 4, Nov. 1996 Page(s):1944 – 1950

[9] Iowa State University's Web Based Voltage Stability Search Engine http://design-2.ece.iastate.edu/biblio/

[10] Guckenheimer, J., Holmes, P.J., *Nonlinear oscillations, dynamical systems, and bifurcation of vector fields*, New York: Springer-Velag, 1983

[11] Illic, M., Zaborsky, J., *Dynamics and control of large electric power systems*, John Wiley & Sons, New York, 2000

[12] Kim, K., Schattler, H., Venkatasubramanian, V., Zaborsky, J., Hirsch, P., "Mehods for calculating oscillations in large power systems," *IEEE Trans. on power systems*, Vol.12, 1997, pp.1639-1648

[13] Rheinboldt, W.C., *Numerical analysis of parameterized nonlinear equations*, New York: John Wiley & Sons, 1986

[14] Souza, De A.C.Z., Canizares, C.A., Quintana, V.H., "New techniques to speed up voltage collapse computations using tangent vectors," *IEEE Trans. on power systems*, Vol.12, 1997, 1380-1387

[15] Dai, R., Rheinboldt, W.C., "On the computation of manifolds of fold-points for parameter-dependent problems," *SIAM J. Numer. Anal.*, Vol. 27, no.2, 1990, pp. 437-446.

[16] Zhou, Y., Ajjarapu, V., "A fast algorithm for identification and tracing of voltage and oscillatory stability margin boundaries," *Proceedings of the IEEE*, Vol. 93, no. 5, 2005, pp.934 – 946

[17] Dobson, I., Lu, L., "Voltage collapse precipitated by the immediate change in stability when generator reactive power limits are encountered," *IEEE Trans. on Circuits and Syst.*,Vol.39:9, pp.762-766, 1992

[18] Anderson, P.M., Fouad, A.A., *Power System Stability and Control*, New York: IEEE PES Press, 1994

[19] Long, B., *The detection of dynamic voltage collapse and transfer margin estimation*, M.S. Thesis, Iowa State University, Ames, IA, 1997

[20] Hill,D. J., Nonlinear dynamic load models with recovery for voltage stability studies, *IEEE Trans. on Power Syst.*, vol.8:1,pp.166-172,1993

[21] Van Cutsem, T., Vournas, C., Voltage stability of electric power systems, Kluwer, 1998

[22] Iba, K., Suzuki, H., Egawa, M., Watanabe, T., *Calculation of critical loading condition with nose curve using homotopy continuation method*, IEEE Transactions on Power Systems, Volume 6, Issue 2, pp.584 – 593, May 1991

[23] Canizares, C. and A., Alvarado, "Point of collapse and continuation methods for large AC/DC power systems," *IEEE Transactions on Power Systems*, vol.8, no.1, February 1993, pp.1-8

[24] Canizares, C. A., Alvarado, F. L., Demarco, C. L., Dobson, I. and Long, W. F., "Point of collapse methods applied to AC/DC power systems," *IEEE Trans. on Power Systems*, vol.7, no.2, pp. 673–683,1992

[25] Chiang, H.D., Flueck, A.J., Shah, K.S., and Balu, N., "CPFLOW: a practical tool for tracing power system steady-state stationary behavior due to load and generation variations,"*IEEE Trans. on power systems*, PWRS-10, May 1995, pp.623-634

[26] Flueck, A.J., Dondeti, J.R., "A new continuation power flow tool for investigating the nonlinear effects of transmission branch parameter variations,"*IEEE Trans. on power systems*, vol.15:1, pp.223-227, 2000

[27] Denis Lee Hau Aik and Anderson, G " Quasi-static stability of HVDC systems considering dynamic effects of synchronous machines and excitation voltage control ," IEEE transactions on Power Delivery , Volume 21, Issue 3, July 2006 pp:1501 – 1514

[28] Canizares, C.A. and Faur, Z.T " Analysis of SVC and TCSC controllers in voltage collapse" IEEE Transactions on Power Systems , Volume 14, Issue 1, Feb. 1999 Page(s):158 – 165

[29] Wen, X., Ajjarapu, V., "Application of a Novel Eigenvalue Trajectory Tracing Method to Identify Both Oscillatory Stability Margin and Damping Margin," IEEE Transactions on Power Systems, Volume 21, May 2006, pp. 817-824

[30] Yang, D. and Ajjarapu, V., "Critical Eigenvalues Tracing for Power System Analysis via Continuation of Invariant Subspaces and Projected Arnoldi Method," to appear in IEEE Trans. on Power Systems